HAL
open science

Lattice QCD at the physical point meets SU(2) chiral perturbation theory

Stephan Durr, Zoltan Fodor, Christian Hoelbling, Stefan Krieg, Thorsten Kurth, Laurent Lellouch, Thomas Lippert, Rehan Malak, Thibaut Métivet, Antonin Portelli, et al.

To cite this version:

Stephan Durr, Zoltan Fodor, Christian Hoelbling, Stefan Krieg, Thorsten Kurth, et al.. Lattice QCD at the physical point meets SU(2) chiral perturbation theory. Physical Review D, 2014, 90 (11), pp.114504. 10.1103/PhysRevD.90.114504 . hal-01258938

HAL Id: hal-01258938

https://hal.science/hal-01258938v1

Submitted on 2 May 2018

HAL is a multi-disciplinary open access archive for the deposit and dissemination of scientific research documents, whether they are published or not. The documents may come from teaching and research institutions in France or abroad, or from public or private research centers.

L'archive ouverte pluridisciplinaire **HAL**, est destinée au dépôt et à la diffusion de documents scientifiques de niveau recherche, publiés ou non, émanant des établissements d'enseignement et de recherche français ou étrangers, des laboratoires publics ou privés.

CPT-P005-2013, WUB/13-14

Lattice QCD at the physical point meets $SU(2)$ chiral perturbation theory

Budapest-Marseille-Wuppertal collaboration

Stephan Dürr[1,2], Zoltán Fodor[1,2,3], Christian Hoelbling[1], Stefan Krieg[1,2], Thorsten Kurth[1], Laurent Lellouch[4,5], Thomas Lippert[2], Rehan Malak[4,5,7], Thibaut Métivet[4,5,8], Antonin Portelli[4,5,6], Alfonso Sastre[4,5], Kálmán Szabó[1]

[1] *Department of Physics, Wuppertal University, Gaussstr. 20, D-42119 Wuppertal, Germany*
[2] *IAS/JSC, Forschungszentrum Jülich, D-52425 Jülich, Germany*
[3] *Inst. for Theor. Physics, Eötvös University, Pázmány P. sét. 1/A, H-1117 Budapest, Hungary*
[4] *Aix Marseille Université, CNRS, CPT, UMR 7332, F-13288 Marseille, France*
[5] *Université de Toulon, CNRS, CPT, UMR 7332, F-83957 La Garde, France*
[6] *School of Physics & Astronomy, University of Southampton, SO17 1BJ, UK*
[7] *CEA/CNRS Maison de la Simulation, USR 3441, CEA-CNRS-INRIA-UPSud-UVSQ, F-91191 Gif-sur-Yvette Cedex, France*
[8] *CEA/IRFU, CEA-Orme des Merisiers, Bât. 703, F-91191 Gif-sur-Yvette Cedex, France*

arXiv:1310.3626v1 [hep-lat] 14 Oct 2013

Abstract

We perform a detailed, fully-correlated study of the chiral behavior of the pion mass and decay constant, based on 2+1 flavor lattice QCD simulations. These calculations are implemented using tree-level, $O(a)$-improved Wilson fermions, at four values of the lattice spacing down to 0.054 fm and all the way down to below the physical value of the pion mass. They allow a sharp comparison with the predictions of $SU(2)$ chiral perturbation theory (χPT) and a determination of some of its low energy constants. In particular, we systematically explore the range of applicability of NLO $SU(2)$ χPT in two different expansions: the first in quark mass (x-expansion), and the second in pion mass (ξ-expansion). We find that these expansions begin showing signs of failure around $M_\pi = 300\,\mathrm{MeV}$ for the typical percent-level precision of our $N_f = 2+1$ lattice results. We further determine the LO low energy constants (LECs), $F = 88.0 \pm 1.3 \pm 0.3$ and $B^{\overline{\mathrm{MS}}}(2\,\mathrm{GeV}) = 2.58 \pm 0.07 \pm 0.02\,\mathrm{GeV}$, and the related quark condensate, $\Sigma^{\overline{\mathrm{MS}}}(2\,\mathrm{GeV}) = (271 \pm 4 \pm 1\,\mathrm{MeV})^3$, as well as the NLO ones, $\bar{\ell}_3 = 2.5 \pm 0.5 \pm 0.4$ and $\bar{\ell}_4 = 3.8 \pm 0.4 \pm 0.2$, with fully controlled uncertainties. Our results are summarized in Table 4. We also explore the NNLO expansions and the values of NNLO LECs. In addition, we show that the lattice results favor the presence of chiral logarithms. We further demonstrate how the absence of lattice results with pion masses below 200 MeV can lead to misleading results and conclusions. Our calculations allow a fully controlled, ab initio determination of the pion decay constant with a total 1% error, which is in excellent agreement with experiment.

Contents

1 Introduction **2**

2 Determination of lattice quantities and associated systematic errors **6**
2.1 Simulation details 6
2.2 Strategy for determining masses and decay constants 7
2.3 Excited state contributions 7
2.4 Lattice spacing 8
2.5 Renormalization 8
2.6 Finite-volume corrections 10
2.7 Illustrative bare results for the basic observables 11

3 Exploring the range of applicability of $SU(2)$ χPT for M_π^2 and F_π **13**
3.1 NLO and NNLO chiral fit strategy 13
3.2 Fit quality and LECs in terms of maximum pion mass for NLO χPT 20
3.3 Fit quality and LECs in terms of maximum pion mass for NNLO χPT 25
3.4 Relative contributions of different orders in χPT and conclusions on its range of applicability 28

4 Results for LECs and other physical quantities **31**

5 On the presence of chiral logarithms and the possible misuse of χPT **36**
5.1 On the presence of NLO chiral logarithms 36
5.2 On the possible misuse of χPT 37

6 Conclusion **42**

Appendices **44**

Appendix A Solution for F_π in the ξ-expansion and ensuing constraints **44**

1 Introduction

The study of the strong interaction at low energy is hampered by the highly nonlinear nature of quantum chromodynamics (QCD). Thus, large scale numerical simulations in lattice QCD have become an essential tool for investigating, from first principles, the nonperturbative dynamics of the theory in that domain. In order to account for all of the relevant physics at the few percent level in low-energy observables, one must include the vacuum fluctuations of the up, down and strange quarks. The heavier quarks contribute corrections in inverse powers of the quark mass squared and of the number of colors, which can be neglected at that level of precision. Moreover, for most QCD observables, isospin breaking effects, which are proportional to powers of the small up-down mass difference, $(m_d - m_u)$, and of the fine structure constant, α, can also be neglected. Thus, today's state-of-the-art calculations are performed with $N_f \geq 2+1$ flavors of sea quarks, where the 2 stands for mass-degenerate u and d quarks with $m_u = m_d = m_{ud} \equiv (m_u + m_d)/2$ and the 1 for a more massive s quark with mass m_s.

One of the main challenges has been to mitigate the fast rising cost of these calculations as the average mass of the simulated up and down quarks is lowered towards its very small physical value, corresponding to a pion mass $M_\pi \simeq 135\,\mathrm{MeV}$. Up until fairly recently, the values of m_{ud} reached were too large to allow a controlled extrapolation of the results to the physical mass point. However, in the last few years, a handful of groups have been able to enter the small mass region, $M_\pi \lesssim 200\,\mathrm{MeV}$, with $N_f \geq 2+1$ [1–8]. In particular, we recently performed $N_f = 2+1$ simulations which reach down to $M_\pi \simeq 120\,\mathrm{MeV}$ (i.e. even below the physical point) on lattices with sizes L up to 6 fm and lattice spacings down to $a \simeq 0.054\,\mathrm{fm}$ [4, 5]. This puts us in a very favorable position to probe the low-energy and low-mass domain of QCD, known as the chiral regime.

In this paper we investigate $SU(2)$ chiral perturbation theory (χPT), which is a systematic expansion around the $m_u = m_d = 0$ chiral limit, at fixed m_s (and possibly $m_c, \dots$) [9,10]. In the corresponding chiral effective Lagrangian there are two low-energy constants (LECs) at leading $O(p^2)$:

$$F \equiv F_\pi\Big|_{m_u,m_d\to 0}\,, \qquad B \equiv -\frac{\langle 0|\bar{u}u|0\rangle}{F_\pi^2}\Big|_{m_u,m_d\to 0}\,, \tag{1}$$

where F_π is the pion, leptonic decay constant, and there are 7 more at next-to-leading $O(p^4)$, denoted by $\ell_i(\mu)$, $i = 1, \dots, 7$ [10]. By definition the LECs are independent of the u and d quark masses, but do depend on the masses of the other four quarks. They also acquire a scale dependence, after renormalization. It is conventional to define them at the renormalization scale $\mu = \hat{M}_{\pi^+} = 134.8(3)\,\mathrm{MeV}$, where $\hat{M}_{\pi^+}$ is the π^+ meson mass, corrected for electromagnetic effects [11]. Up to negligible corrections, it is also equal to $\bar{M}_\pi$, the pion mass in the isospin limit ($m_u - m_d \to 0$ at fixed m_{ud}) [11], in which our $N_f = 2+1$ lattice calculations are performed.

The observables which we consider here are M_π^2 and F_π. Their expansions in powers of the quark mass are known to next-to-next-to-leading order (NNLO) in the $SU(2)$ chiral effective theory. In the isospin limit, the explicit expressions may be written in the form[1], $m_u = m_d = m_{ud}$ [12]

$$\begin{aligned} M_\pi^2 &= M^2\left\{1 - \frac{1}{2}x\ln\frac{\Lambda_3^2}{M^2} + \frac{17}{8}x^2\left(\ln\frac{\Lambda_M^2}{M^2}\right)^2 + x^2 k_M + O(x^3)\right\}, \\ F_\pi &= F\left\{1 + x\ln\frac{\Lambda_4^2}{M^2} - \frac{5}{4}x^2\left(\ln\frac{\Lambda_F^2}{M^2}\right)^2 + x^2 k_F + O(x^3)\right\}. \end{aligned} \tag{2}$$

The expansion parameter is given by

$$x = \frac{M^2}{(4\pi F)^2}, \qquad M^2 = 2Bm_{ud} = \frac{2m_{ud}\Sigma}{F^2}. \tag{3}$$

The $O(p^6)$ LECs, k_M and k_F, in Eq. (2) are also independent of the u and d quark masses. The scales in the quadratic logarithms can be written in terms of $O(p^4)$ LECs through:

$$\begin{aligned} \ln\frac{\Lambda_M^2}{M^2} &= \frac{1}{51}\left(60\ln\frac{\Lambda_{12}^2}{M^2} - 9\ln\frac{\Lambda_3^2}{M^2} + 49\right), \\ \ln\frac{\Lambda_F^2}{M^2} &= \frac{1}{30}\left(30\ln\frac{\Lambda_{12}^2}{M^2} + 6\ln\frac{\Lambda_3^2}{M^2} - 6\ln\frac{\Lambda_4^2}{M^2} + 23\right), \end{aligned} \tag{4}$$

[1] Here and in the following, we work in the normalization $F_\pi \equiv f_\pi/\sqrt{2} = 92.2\mathrm{MeV}$.

where we have defined $\ln \Lambda_{12}^2 = (7 \ln \Lambda_1^2 + 8 \ln \Lambda_2^2)/15$. The logarithmic scales Λ_n in Eqs. (2)–(4) are related to the effective coupling constants $\bar{\ell}_3, \bar{\ell}_4$ of the chiral Lagrangian at running scale $\hat{M}_{\pi^+}$ through:

$$\bar{\ell}_n = \ln \frac{\Lambda_n^2}{\hat{M}_{\pi^+}^2}, \quad n = 1, ..., 7 \;\&12 \;, \tag{5}$$

where we have generalized the definition to also include Λ_{12} and $\bar{\ell}_{12}$.

It is interesting to note that once we fix Λ_3 and Λ_4, which appear already at NLO in the expansions of F_π and M_π, the new logarithmic scales Λ_M and Λ_F are linearly related. This reduces from 8 to 7 the number of parameters in a combined fit of the dependence of M_π^2 and F_π on m_{ud}. In particular this means that with precise enough lattice results for the pair (M_π^2, F_π), at four or more values of m_{ud}, one can in principle determine the 7 independent LECs which appear in the expansions of Eq. (2) as well as test the compatibility of the lattice results with NNLO χPT. Such an NNLO analysis is still very demanding by today's standards.

The situation is significantly more simple if the expressions of Eq. (2) are truncated at NLO. Then, only 4 LECs appear, B and F at $O(p^2)$, and $\bar{\ell}_3$ and $\bar{\ell}_4$ at $O(p^4)$. This is the expansion considered in previous $N_f \geq 2+1$ work [2,6,7,13–20]. Of those, the only calculation whose simulations reach all the way down to the physical up-down quark mass is [6]. In that work, NNLO effects are also investigated.

Work on the x-expansion has also been performed using $N_f = 2$ lattice QCD simulations in [21–29]. Such work has provided interesting information about $SU(2)$ χPT. However, because the effects of the omitted strange, sea quark in these calculations cannot be quantified *a priori*, the conclusions which are drawn from such studies will differ qualitatively and quantitatively from ours by an unknown amount. Thus, we do not consider them further here and refer the interested reader to [11] and the original papers for further information.

As with any expansion, the chiral expressions can be reorganized in terms of any other parameter which is related to x of Eq. (3), through a power series in x. In particular, one can invert Eq. (2), and express M and F as an expansion in

$$\xi \equiv \frac{M_\pi^2}{(4\pi F_\pi)^2} \;. \tag{6}$$

The corresponding expressions read [11]

$$\begin{aligned} M^2 &= M_\pi^2 \left\{ 1 + \frac{1}{2}\xi \ln \frac{\Lambda_3^2}{M_\pi^2} - \frac{5}{8}\xi^2 \left(\ln \frac{\Omega_M^2}{M_\pi^2} \right)^2 + \xi^2 c_M + O(\xi^3) \right\} \;, \\ F &= F_\pi \left\{ 1 - \xi \ln \frac{\Lambda_4^2}{M_\pi^2} - \frac{1}{4}\xi^2 \left(\ln \frac{\Omega_F^2}{M_\pi^2} \right)^2 + \xi^2 c_F + O(\xi^3) \right\} \;. \end{aligned} \tag{7}$$

This expansion has the advantage that its parameter ξ is given in terms of the physical mass and decay constant of the particle which is actually contributing to the process. Thus, it resums a number of higher-order contributions which are known to be present, and therefore might exhibit better convergence. In Eq. (7), the scales of the quadratic logarithms are determined by $\Lambda_1, \ldots, \Lambda_4$ [11]:

$$\ln \frac{\Omega_M^2}{M_\pi^2} = \frac{1}{15} \left(60 \ln \frac{\Lambda_{12}^2}{M_\pi^2} - 33 \ln \frac{\Lambda_3^2}{M_\pi^2} - 12 \ln \frac{\Lambda_4^2}{M_\pi^2} + 52 \right) \;, \tag{8}$$

$$\ln \frac{\Omega_F^2}{M_\pi^2} = \frac{1}{3}\left(-15 \ln \frac{\Lambda_{12}^2}{M_\pi^2} + 18 \ln \frac{\Lambda_4^2}{M_\pi^2} - \frac{29}{2}\right) .$$

Here we study $SU(2)$ χPT in both the x and ξ-expansions. While most of the work concerns the NLO expansions, we also investigate the NNLO expansions, in particular in regards to its range of applicability.

The remainder of the paper is organized as follows. In Sec. 2 we detail the lattice ensembles used in the present study and the various steps in required to determine the chiral observables M_π, F_π and the quark masses from our correlation functions. We also discuss how we perform the necessary renormalizations and how we account for the various sources of lattice systematic errors in our analyses. In Sec. 3, we systematically explore the range of applicability, in pion or light-quark mass, of the various $SU(2)$ χPT expressions for $M_\pi^2/2m_{ud}$ and F_π. In particular, we assume that $SU(2)$ χPT is valid around $M_\pi^{\rm ph}$, where here and below the superscript "ph" stands for "physical" or from experiment, and explore how far up one can go in pion or light-quark mass, while still maintaining an acceptable description of the lattice results. Then, having established the range of applicability of $SU(2)$ χPT for $M_\pi^2/2m_{ud}$ and F_π, we devote Sec. 4 to a determination of the corresponding LO, NLO and NNLO LEC's, as well as of F_π and the quark condensate. In particular, we perform a complete systematic error analysis for these quantities. Our main results are summarized in Table 4. In Sec. 5 we show that the lattice results favor the presence of chiral logarithms. We also show how the absence of lattice results with $M_\pi \leq 200\,\text{MeV}$ can lead to misleading results and conclusions. In the paper's final section, Sec. 6 we present our conclusions. We also provide an appendix in which we discuss our implementation of the ξ-expansion and the ensuing constraints on the LECs.

2 Determination of lattice quantities and associated systematic errors

In this section, we describe how we compute the values of M_π, F_π and m_{ud} required for the χPT studies described below. We do so for a range of m_{ud} around and above its physical value to explore the range of applicability of $SU(2)$ χPT. We also do so for a large variety of lattice parameters to be able to control all sources of systematic uncertainties.

As first proposed in [1], we determine the central values, statistical and systematic uncertainties of our results from histograms obtained by combining the results form a variety of different analyses. Indeed, for each step of the analysis, we consider a wide range of possible procedures whose effects we propagate to the end of the calculation. Thus, our analyses form a tree where each path corresponds to one of the many different possible ways in which to compute a given observable.

The trunk of the tree corresponds to the primary observables. In the present study, they are the hadron correlators. Thus, the first level of branching occurs in choosing the time interval over which these correlators are fitted to obtain the bare masses and decays constants in lattice units. The next level of branching is a result of the different ways which we have to set the lattice spacing. Note that at each level, these same twigs are sprouted from every branch. For quantities which require renormalization, an additional level of branching arises, corresponding to the different ways which we have to compute the renormalization constants. Note that the renormalization constants are themselves the result of a tree, as described below.

At that stage in the analysis, we have obtained, in all possible ways, the renormalized results in physical units for each simulation, which we will need to study $SU(2)$ χPT. Note that throughout our analysis we fully take into account statistical correlations as well as correlations induced by quantities such as the lattice spacing or the renormalization constants, which are shared by all ensembles at a given β.

In the remainder of the section, we detail the ingredients of the analysis briefly described here, including the procedure used to determine the associated systematic uncertainties.

2.1 Simulation details

The study presented here is based on the forty-seven $N_f = 2+1$ ensembles that we produced for determining the light quark masses [4, 5]. They were generated using a tree-level $O(a^2)$-improved Symanzik gauge action [30–33], together with tree-level clover-improved Wilson fermions [34], coupled to links which have undergone two levels of HEX smearing [35–37]. Details of the action and simulations are given in [5]. Here we mention that we use the 26 large-volume ensembles that were generated at 4 values of the lattice spacing spanning the range $0.054\,\text{fm} \lesssim a \lesssim 0.093\,\text{fm}$. We found that the low momentum cutoff of the coarsest lattice in [5], with $a = 0.116\,\text{fm}$, does not allow a precise determination of the renormalization constant of the axial current, Z_A, required for the computation of F_π. The uncertainty associated with its determination, of order 1.5%, is sufficiently large that it negates any improvement the inclusion of the results at that lattice spacing could bring to the final results. Thus, as in [38], we have chosen not to incorporate the results of this simulation in our analysis.

The strange quark mass in these simulations is varied around the physical value to allow for a precise interpolation to that value. For the 2 lattice spacings $a \approx 0.077$, $0.093\,\text{fm}$, simulations were performed all the way down to the physical value of m_{ud} and even below.

For the remaining 2 lattice spacings ($a \approx 0.065$, 0.054 fm), the pion masses reached are 180 and 220 MeV, respectively. Thus, our simulations allows us to replace the usual extrapolations to physical m_{ud} by an interpolation, but also to systematically probe the $SU(2)$ chiral regime.

The parameters of the simulations used in this work are summarized in Tables 1 and 2, together with illustrative results for the lattice spacing, renormalization constants and observables that are discussed below.

2.2 Strategy for determining masses and decay constants

We determine aM_π and aF_π/Z_A for each simulation point by performing a combined correlated fit of the asymptotic time behavior of the two, zero-momentum correlators, $\sum_{\vec{x}}\langle A_0^L(\vec{x}, x_0)P^{G\dagger}(0)\rangle$ and $\sum_{\vec{x}}\langle P^G(\vec{x}, x_0)P^{G\dagger}(0)\rangle$, to the appropriate asymptotic forms. Here A_0 is the time-component of the axial-vector current and P is the corresponding pseudoscalar density. Both are appropriately tree-level $O(a)$-improved [34, 39]. These operators have the flavor quantum numbers appropriate for annihilating a π^+. The superscript L stands for "local" (i.e. all quark fields are at the same spacetime point) and G for "Gaussian". Indeed, to reduce the relative weight of excited states in the correlation functions, Gaussian sources and sinks are used (except for the axial current, of course), with a radius of about 0.32fm, which was found to be a good choice [1]. The kaon masses, aM_K, are obtained from a correlated fit to the corresponding, two-point, pseudoscalar density correlators.

To study the x-expansion discussed above, we need to determine the quark masses m_{ud} and m_s for each simulation point. Here we follow the $O(a)$-improved ratio-difference method put forward in [4, 5]. Thus, for each simulation point we determine the bare axial-Ward-identity mass combinations $2m_{ud}^{\rm PCAC}(g_0) = (m_u+m_d)^{\rm PCAC}(g_0)$ and $(m_s+m_{ud})^{\rm PCAC}(g_0)$ from the relevant ratio of two-point functions, $\partial_0 \sum_{\vec{x}}\langle A_0^L(\vec{x}, x_0)P^{G\dagger}(0)\rangle \ / \ \sum_{\vec{x}}\langle P^G(\vec{x}, x_0)P^{G\dagger}(0)\rangle$, where ∂_μ is the symmetric derivative. The operators are appropriately tree-level $O(a)$-improved. From this we obtain the ratio of renormalized, improved quark masses, $r^{\rm imp} \equiv m_s^{\rm AWI}(\mu)/m_{ud}^{\rm AWI}(\mu)$, through $r^{\rm imp} = m_s^{\rm PCAC}(g_0)/m_{ud}^{\rm PCAC}(g_0)[1 + O(a)]$, where the $O(a)$ improvement terms are given in [5] and μ is a renormalization scale. Because the numerator and denominator in this ratio renormalize identically, all scale and scheme dependence cancels. This ratio is then combined with the difference of renormalized, improved vector-Ward-identity masses, $(m_s - m_{ud})^{\rm VWI}(\mu) = d^{\rm imp}(g_0)/(aZ_S(a\mu, g_0))$, to obtain the renormalized values $m_{ud}(\mu)$ and $m_s(\mu)$ of the quark masses for a given simulation. Here $d^{\rm imp}(g_0) = (am_s^{\rm bare} - am_{ud}^{\rm bare})(g_0)[1+O(a)]$, where the $O(a)$ improvement terms are also given in [5] and where $am_{ud,s}^{\rm bare}(g_0)$ are the bare lagrangian masses used at bare coupling g_0. In the definition of the mass difference, $Z_S(a\mu, g_0)$ is the renormalization constant of the non-singlet scalar density in any chosen scheme at scale μ [4,5]. Here we will mainly use its renormalization group invariant (RGI) value, which is regularization scheme and renormalization scale independent.

2.3 Excited state contributions

A source of uncertainty, which often proves important, is the contamination by excited states of the desired ground state in two-point correlators. As described above, this contamination is reduced by working with extended sources and sinks. Moreover, we tested 1-state and 2-state fits, and found complete agreement if the 1-state fits start at $t_{\rm min}\simeq 0.7$ fm for the pseudoscalar meson channels and from $t_{\rm min}\simeq 0.8$ fm for the Ω. In lattice units this amounts to $at_{\rm min} = \{8,$

$9, 11, 13\}$ for β=$\{3.5, 3.61, 3.7, 3.8\}$ (and $\sim$20% later for baryons). In order to estimate any remaining excited state effects, we repeat our analysis with an even more conservative fit range, starting at $at_{\rm min}$=$\{9, 11, 13, 15\}$ for mesons and $\sim$ 20% later for baryons. The end of the fit interval is always chosen to be $at_{\rm max} = 2.7\times at_{\rm min}$ or $T/2 - 1$ for lattices with a time extent shorter than $5.4\times at_{\rm min}$. In total, this yields 2 combined, time-fit intervals.

2.4 Lattice spacing

To set the lattice spacing, we follow [1] and use the Ω baryon mass. Thus, we perform a combined interpolation to the physical mass point of our results for aM_Ω at all four values of β, with the following functional form:

$$aM_\Omega = aM_\Omega^{\rm ph}(\beta) \quad \left\{1 + c_s\left[\left(\frac{aM_{s\bar{s}}}{aM_\Omega}\right)^2 - \left(\frac{M_{s\bar{s}}}{M_\Omega}\right)^2_{\rm ph}\right] + c_{ud}\left[\left(\frac{aM_\pi}{aM_\Omega}\right)^2 - \left(\frac{\hat{M}_{\pi^+}}{M_\Omega}\right)^2_{\rm ph}\right]\right\} , \tag{9}$$

where $(M_{s\bar{s}})^2 = 2M_K^2 - M_\pi^2$. In (9), there is of course one parameter $aM_\Omega^{\rm ph}$ per lattice spacing, but we find that our fits do not require the parameters $c_{s,ud}$ to be β dependent. Moreover, for the range of quark masses considered, we find that we do not need higher order terms in the mass expansion. Thus, these fits have a total of 7 parameters.

To estimate the systematic uncertainties in our final results associated with the determination of the lattice spacing, we consider $2 \times 2 = 4$ different procedures for its computation, which we propagate throughout our analysis. In particular, we consider 2 different time-fitting ranges for the extraction of aM_Ω in each simulation ($at_{\rm min}$=$\{10, 11, 13, 16\}$ or $at_{\rm min}$=$\{11, 13, 16, 18\}$ for β=$\{3.5, 3.61, 3.7, 3.8\}$) to estimate the possible effects of excited state contributions to the two-point functions and 2 pion cuts in the mass interpolation fits described above (380 or 480 MeV), to estimate the uncertainties associated with the interpolation of aM_Ω to the physical mass point. This gives us a total of 4 values of the lattice spacing for each β. While each of these procedures enters individually in our determination of systematic uncertainties for all quantities which depend on the lattice spacing, we give in Table 1 illustrative numbers, whose central values are the fit-quality weighted averages of the results from the different procedures and whose statistical errors are the variance of these central values over 2000 bootstrap samples. The systematic errors are obtained from the variance over the procedures.

2.5 Renormalization

To determine the renormalization constants we use the nonperturbative renormalization and running techniques developed in [4, 5, 40], which are based on the RI/MOM methods *à la Rome-Southampton* [41]. For Z_S, we follow [5] and Z_A is determined as in [38]. As described in [5], the calculation of these constants is performed using 20 fully independent $N_f = 3$ simulations at the same four values of β as the $N_f = 2 + 1$ production runs.

In order to compute the systematic uncertainties associated with renormalization on our final results, we consider 6 different procedures for the determination of Z_S and 3 for Z_A, as described in detail [5] and [38], respectively. Here we simply outline the different procedures.

The renormalization of quark masses is performed in three steps [5]. We first compute Z_S in a MOM scheme at an intermediate scale μ', which is low enough that discretization errors

β	a [fm]	$1/Z_S^{\rm RGI}$	Z_A
3.5	0.0904(10)(2)	1.47(2)(3)	0.9468(5)(56)
3.61	0.0755(11)(3)	1.50(3)(2)	0.9632(4)(53)
3.7	0.0647(11)(3)	1.54(3)(3)	0.9707(3)(35)
3.8	0.0552(8)(1)	1.58(1)(1)	0.9756(1)(15)

Table 1: Illustrative results for the lattice spacing and the renormalization constants at our four values of β. $1/Z_S^{\rm RGI}$ is required to convert bare quark masses to masses renormalized in the $N_f = 3$ RGI scheme. To convert results to the $\overline{\rm MS}$ scheme at scale 2 GeV, the numbers in the third column of the table must be multiplied by 0.750 [5]. Z_A is used to correctly normalize F_π. In the results above, the first error is statistical and the second is systematic. The main text explains how these errors are obtained as well as why the results cannot be used to reproduce the extensive analyses performed in this paper.

on the renormalization constant are under control. We then run the results nonperturbatively in that scheme up to a fully perturbative scale $\mu = 4$ GeV where they are converted nonperturbatively to the usual massless, $N_f = 3$, RI/MOM scheme. Values in other schemes are then obtained using renormalization-group-improved perturbation theory at $O(\alpha_s^3)$ [42], with negligible uncertainty. These three steps lead to 6 procedures in the following way. In step 1 we consider three different MOM schemes to determine the uncertainties associated with the choice of an intermediate scale μ' and with the chiral extrapolation required to define the RI/MOM scheme. These correspond to the scale and quark-mass pairs, μ'[GeV], $m_{\rm ref}^{\rm RGI}$[MeV] $= \{\{2.1, 0\}, \{2.1, 70\}, \{1.3, 70\}\}$. The additional factor of two comes from the two ways in which we continuum extrapolate the nonperturbative running and matching factors, either assuming that the $O(\alpha_s a)$ or $O(a^2)$ terms dominate.

Z_A is a finite renormalization and therefore does not have a scale or scheme dependence. Nevertheless, we must find a window, at large values of the squared-momentum, $p^2 \gg \Lambda_{\rm QCD}$, of the quark three-point function used to determine Z_A, in which this correlation function is approximately constant. For such momenta the correlation function is dominated by perturbation theory and allows for a reliable extraction of Z_A. To estimate the uncertainties associated with the choice of this window and with possible $(ap)^2$ discretization corrections, we fit our results for the relevant three-point function to the functional form $Z_A + A(am_q) + B(ap)^2$ for three different ranges in p^2. Here, am_q is the common, $N_f = 3$, bare PCAC mass. For all four β these ranges begin either at $p^2 = 3.35$, 4.37 or 5.52 GeV^2. These values of p^2 are large enough that we are not sensitive to subleading OPE contributions proportional to inverse powers of p^2. The upper bounds of the fit ranges are chosen to be $1.5/a$ in all cases. This is below $\pi/(2a)$ which we found in [5] is a region in which discretization errors on the RI/MOM correlation functions are subdominant.

We provide in Table 1 illustrative results for $1/Z_S^{\rm RGI}$ and Z_A for the four values of the lattice spacing used in our study. Their central values are the fit quality weighted averages of the results from the different procedures and their statistical errors are the variance of these central values over 2000 bootstrap samples. Their systematic uncertainties are obtained from the variance over the different procedures.

The results for a, $1/Z_S$ and Z_A in Table 1 are only illustrative, because they cannot be naively combined with the observables given Table 2 to perform a fully self-consistent analysis such as the one presented below. Indeed in our analysis, the statistical and systematic

uncertainties associated with these quantities are propagated in a fully-consistent manner to our final results by including them in our resampling and systematic error loops. Such an analysis requires having the full statistical and systematic error distributions of the quantities in Tables 2 and 1, as well as their correlations.

2.6 Finite-volume corrections

Because our calculations are performed in large but finite boxes, our results for F_π and M_π suffer from finite-volume corrections. These effects have been determined at one loop in $SU(2)$ χPT in [43]. In [44] they have been computed to three loops for M_π and two loops for F_π, up to negligibly small exponential corrections. Since the expressions for the latter involve $O(p^4)$ LECs at two loops, some of which we cannot self-consistently determine here, we prefer to rely on the one-loop formulae, which can be written in terms of quantities which we calculate directly. The difference is a correction on an already small correction.

In the ξ-expansion, the one-loop finite-volume corrections are given by [43]:

$$\frac{M_\pi^2(L)}{M_\pi^2} - 1 = \frac{1}{2}\xi\, \tilde{g}_1(M_\pi L) + O\left(\xi^2\right) \tag{10}$$

$$\frac{F_\pi(L)}{F_\pi} - 1 = -\xi\, \tilde{g}_1(M_\pi L) + O\left(\xi^2\right) \tag{11}$$

where ξ is defined in Eq. (6). Analogous results are obtained for the x-expansion. The shape function $\tilde{g}_1(x)$ has a well behaved large-argument expansion in terms of Bessel functions of the second kind, which themselves can be expanded asymptotically:

$$\tilde{g}_1(x) \overset{x\to\infty}{\sim} \frac{24K_1(x)}{x} + \frac{24K_2(\sqrt{2}x)}{\sqrt{2}x} + \cdots \tag{12}$$

$$K_\nu(x) \overset{x\to\infty}{\sim} \left(\frac{\pi}{2x}\right)^{1/2} \exp(-x)\left[1 + \frac{4\nu^2-1}{8x} + \cdots\right] . \tag{13}$$

In a first instance, we include the corrections of Eq. (11) (and the corresponding ones in the x-expansion), directly into the fit functions given in Eq. (15) (and in Eq. (14) for the x-expansion). We find that the subtraction of finite-volume effects on F_π significantly improves the fit quality. The corrections on M_π^2, which are four times as small and significantly smaller than statistical errors, do not improve the χ^2 of the fits nor do they change the results.

For our simulation parameters, the one-loop finite-volume effects on F_π are typically 0.5% and never exceed 1.1%. Thus, higher-order corrections are expected to be much smaller than our statistical errors. To check this, we perform a second set of fits in which we multiply the RHSs of each of the two equations in (11) (and the equivalent expressions in the x-expansion) by a coefficient which is treated as an additional free parameter in these fits. Thus, each of our ξ and x-expansion fits have two additional parameters. These parameters are 1 if the NLO estimate of finite-volume corrections is exact.

In practice, for NLO fits in the important region $M_\pi \leq 300\,\mathrm{MeV}$, we find that the addition of these parameters does not improve the quality of the fits. Moreover, the uncertainties on the coefficients come out very large–between 80 and 90% depending on the quantity and the expansion–and the coefficients themselves are consistent with 1 within at worst 1.2 standard deviations. Finally, the results obtained for the LECs are consistent, within statistical errors,

with those obtained using the analytic finite-volume expressions, and none of the conclusions that we draw below are modified.

In light of these findings and of the expectation that higher-order, finite-volume corrections are negligible compared to our statistical errors, we have decided to fix the finite-volume corrections to their NLO values in our analysis, so as not to artificially increase our statistical errors by adding two irrelevant parameters.

2.7 Illustrative bare results for the basic observables

To conclude this section, we tabulate our simulation points, together with the corresponding values of $Z_S \times am_{ud}$, $aM_{s\bar{s}} \equiv [2(aM_K)^2 - M_\pi^2]^{1/2}$, aM_π and aF_π/Z_A. They are given in Table 2. $Z_S \times am_{ud}$ is the bare, subtracted value of the average up-down quark mass given by the ratio-difference method described in Sec. 2.2, before the final multiplicative renormalization. The quantities in Table 2 are the basic observables needed to study the chiral behavior of M_π^2 and F_π. Their central values are the fit quality weighted averages of the results from the two different time-fit ranges of the correlation functions and their statistical errors are the variance of these central values over 2000 bootstrap samples. Their systematic uncertainties are obtained from the variance over the two procedures.

These values are only meant as illustrative. In particular, they do not include a description of statistical and systematic error correlations, including those with the lattice spacing. While this seriously limits the reliability of any conclusion drawn from them, we give them nonetheless so that the interested readers may get their own sense of what sort of chiral behavior these results allow, after combining them with the values of the lattice spacing a and the renormalization constants $1/Z_S$ and Z_A given in Table 1.

β	$T \times L^3$	$am_{ud}^{\rm bare}$	$am_s^{\rm bare}$	$Z_S(am_{ud})$	$aM_{s\bar{s}}$	aM_π	aF_π/Z_A
	48×24^3	-0.041	-0.006	0.01475(33)	0.3415(5)(2)	0.19188(50)(6)	0.05491(34)(0)
	48×24^3	-0.0437	-0.006	0.01188(27)	0.3396(5)(2)	0.17238(49)(3)	0.05263(34)(0)
	64×24^3	-0.041	-0.012	0.01428(33)	0.3175(95)(4)	0.18790(90)(30)	0.05384(84)(6)
	64×32^3	-0.0463	-0.012	0.00853(20)	0.3134(10)(7)	0.14440(70)(60)	0.05004(62)(6)
3.5	64×32^3	-0.048	-0.0023	0.00726(17)	0.3496(75)(5)	0.13480(70)(20)	0.04982(59)(1)
	64×32^3	-0.049	-0.006	0.00579(15)	0.3339(10)(5)	0.12100(9)(3)	0.04837(84)(3)
	64×32^3	-0.049	-0.012	0.00560(14)	0.3103(69)(9)	0.11733(64)(3)	0.04800(68)(2)
	64×48^3	-0.0515	-0.012	0.00288(7)	0.3079(9)(1)	0.08410(60)(20)	0.04628(58)(3)
	64×64^3	-0.05294	-0.006	0.00149(5)	0.3281(9)(5)	0.06126(60)(9)	0.04440(75)(6)
	48×32^3	-0.028	0.0045	0.01008(23)	0.2955(6)(3)	0.14852(49)(2)	0.04408(34)(2)
	48×32^3	-0.03	0.0045	0.00808(18)	0.2929(7)(3)	0.13217(50)(9)	0.04262(39)(1)
	48×32^3	-0.03	-0.0042	0.00783(18)	0.2602(7)(2)	0.12943(59)(4)	0.04207(39)(1)
3.61	48×48^3	-0.03121	0.0045	0.00678(15)	0.2926(6)(2)	0.12096(30)(3)	0.04234(25)(2)
	48×48^3	-0.033	0.0045	0.00490(12)	0.2909(9)(3)	0.10251(48)(7)	0.04005(37)(1)
	48×48^3	-0.0344	0.0045	0.00344(8)	0.2907(10)(4)	0.08610(6)(2)	0.03921(38)(6)
	72×64^3	-0.0365	-0.003	0.00096(3)	0.2592(10)(5)	0.04646(5)(3)	0.03583(62)(0)
	64×32^3	-0.0208	0.0	0.00821(19)	0.2276(13)(2)	0.12455(11)(1)	0.03660(57)(1)
	64×32^3	-0.0208	0.001	0.00831(19)	0.2328(10)(2)	0.12491(10)(1)	0.03607(56)(1)
3.7	64×32^3	-0.0208	-0.005	0.00823(19)	0.2082(7)(1)	0.12489(64)(8)	0.03588(42)(0)
	64×48^3	-0.0254	0.0	0.00354(8)	0.2259(9)(3)	0.08168(55)(2)	0.03304(41)(2)
	64×48^3	-0.0254	-0.005	0.00348(8)	0.2043(6)(3)	0.08046(4)(2)	0.03270(51)(2)
	64×64^3	-0.027	0.0	0.00196(5)	0.2235(52)(5)	0.06029(30)(9)	0.03303(44)(3)
	64×32^3	-0.0148	0.0	0.00915(21)	0.1898(10)(3)	0.12052(12)(3)	0.03123(63)(1)
3.8	64×48^3	-0.019	0.0	0.00422(9)	0.1873(13)(2)	0.08184(11)(0)	0.02814(49)(1)
	64×48^3	-0.019	0.003	0.00423(10)	0.2010(11)(1)	0.08261(14)(1)	0.02784(47)(3)
	144×64^3	-0.021	0.0	0.00221(5)	0.1879(80)(6)	0.05981(25)(1)	0.02688(59)(1)

Table 2: Parameters of the simulations used in this work and illustrative results for the quantities $Z_S(am_{ud})$, $aM_{s\bar{s}}$, aM_π and aF_π/Z_A. In these results, the first error is statistical and the second is systematic, and they are obtained as described in the text. For $Z_S(am_{ud})$, the systematic error is 0 for the number of digits given and is not reported.

3 Exploring the range of applicability of $SU(2)$ χPT for M_π^2 and F_π

In this section we explore the range of applicability of $SU(2)$ χPT, in u-d and pion mass, for the various expansions discussed in Sec. 1. We proceed in a systematic fashion. We begin by assuming that χPT is valid around $M_\pi^{\rm ph}$, the experimental value of M_π, where we have our lightest points. We then study the p-values of the *combined, fully-correlated* fit of the different chiral expansions to our results for F_π and M_π^2 with $m_{ud} \leq m_{ud}^{\rm max}$ or $M_\pi \leq M_\pi^{\rm max}$, as $m_{ud}^{\rm max}$ or $M_\pi^{\rm max}$ is increased. Because our procedure correctly accounts for all correlations in the lattice observables, the p-value is a meaningful quantity whose value indicates the probability that randomly chosen results consistent with the chiral forms would give a worse fit. Thus we expect the p-value to drop as $m_{ud}^{\rm max}$ or $M_\pi^{\rm max}$ is increased beyond the range of applicability of a given $SU(2)$ χPT expansion for F_π and M_π^2. It is important to note, however, that the sharpness of the drop and the conclusions which can be drawn depend on the size of the error bars on the quantities studied.

In order to carry this program out on our simulation results, there are two topics which we must address. The first is the dependence of M_π^2 and F_π on strange-quark mass. In our $N_f = 2+1$ simulations, we vary m_s in the vicinity of its real-world value to allow us to tune it precisely to that value in our final results. To parametrize this mass dependence we follow [45] for instance, and expand the LECs of $SU(2)$ χPT in power series in the strange quark mass, or an equivalent variable such as $M_{s\bar{s}}^2 \equiv 2M_K^2 - M_\pi^2$, around the physical strange quark point. Since these corrections are small, they are usually only visible in the LO terms of the chiral expansion. For instance, terms of order x or ξ times $(m_s - m_s^{\rm ph})/M_{\rm QCD}$, where $M_{\rm QCD}$ is a scale characteristic of QCD (e.g. the ρ-meson mass M_ρ), are not detectable at our level of precision. We will retain only those terms whose coefficients differ from zero by more than one standard deviation in our fits.

The second point that must be addressed is that of discretization errors. At finite lattice spacing, results for M_π, F_π and the renormalized quark masses suffer from discretization errors which are proportional to powers of a, up to logarithms. Because the fermion action that we use is tree-level $O(a)$-improved, the leading such errors are formally proportional to $\alpha_s(a)a$. However, at our coarsest lattice spacing, terms proportional to a^2 may be dominant. Thus, we consider both possibilities in our analysis. We find that our fits work better if we consider that discretization errors are associated with a given lattice quantity and consistently include the required corrections every time that quantity appears. This is what is done in (14) for m_{ud}, for instance. In fact, we performed an extensive study of these effects and found that the only discretization corrections which our results are sensitive to are $\alpha_s a$ or a^2 corrections in m_{ud}. Attempts to add discretization corrections to M_π or F_π always lead to coefficients which were consistent with zero within less than one standard deviation. Thus, in the sequel, we keep only discretization corrections on the light-quark mass.

3.1 NLO and NNLO chiral fit strategy

Combining the strange-quark-mass and lattice-spacing dependencies, discussed above, with the $SU(2)$ chiral expansions of Sec. 1 gives the desired NLO and NNLO parametrizations. At NLO in the x-expansion, we obtain the following expressions for the lattice quantities

$(aM_\pi)^2/2(am_{ud})$, (aF_π), am_{ud}, $(aM_{s\bar{s}})^2$, a, Z_A and Z_S:

$$\begin{aligned}\frac{(aM_\pi)^2}{2(am_{ud})} &= \frac{a^p}{Z_S^p}(1-\gamma_1^a f(a^p)+\gamma_1^s(\Delta M_{s\bar{s}}^2)^p)(B_\pi^{x-\mathrm{NLO}})(m_{ud}^p;B,F,\bar{\ell}_3)\,,\\ (aF_\pi) &= \frac{a^p}{Z_A^p}(1+\gamma_2^s(\Delta M_{s\bar{s}})^2)F_\pi^{x-\mathrm{NLO}}(m_{ud}^p;B,F,\ell_4)\,,\end{aligned} \tag{14}$$

$$(am_{ud}) = a^p Z_s^p(1+\gamma_1^a f(a^p))m_{ud}^p\,,\quad (aM_{s\bar{s}})^2 = (a^p)^2(M_{s\bar{s}}^2)^p\,,$$
$$a = a^p\,,\quad Z_A = Z_A^p\,,\quad Z_S = Z_S^p,$$

where $(aM_{s\bar{s}})^2 \equiv 2(aM_K)^2-(aM_\pi)^2$, $(\Delta M_{s\bar{s}}^2)^p \equiv (M_{s\bar{s}}^2)^p - M_{s\bar{s}}^{\mathrm{ph}}$ and $f(a)=\alpha_s(a)\,a$ or a^2, depending on which discretization errors are chosen as leading. $B_\pi^{x-\mathrm{NLO}}(m_{ud}^p;B,F,\bar{\ell}_3)$ is B times the NLO part of the expression in brackets on he RHS of the first equation in (2) and $F_\pi^{x-\mathrm{NLO}}(m_{ud}^p;B,F,\ell_4)$ are the NLO expressions of Eq. (2). The relevant chiral parameters of the fit are the 2 LO LECs, B and F, and the 2 NLO LECs, $\bar{\ell}_3$ and $\bar{\ell}_4$. There are also a discretization parameter, γ_1^a, and the strange-mass dependence parameters γ_1^s and γ_2^s. An extensive study of these two effects showed that the only relevant ones are those given by γ_1^a, γ_1^s and γ_2^s.

In Eq. (14), variables with a superscript p are also parameters of the fit. These are associated with the corresponding lattice quantities. As in our previous work, they are added so that uncertainties and correlations in all lattice quantities, including those which appear in nontrivial expressions involving the parameters, can consistently be accounted for in the χ^2. Since there is one such variable per new observable added, the total number of d.o.f. is unchanged.

For each β we define the large lattice data vector $y^T(\beta) = (a, Z_A, Z_S, am_{ud}, (aM_{s\bar{s}})^2, 2(am_{ud})/(aM_\pi)^2, (aF_\pi), \cdots)$ where the quantities am_{ud}, $(aM_{s\bar{s}})^2$, $2(am_{ud})/(aM_\pi)^2$, (aF_π) are repeated for every simulation at that lattice spacing. We then use a bootstrap to compute a correlation matrix $C_{ij}(\beta)$ for each β between different components i and j of the vector y. Because simulations are independent, this matrix is essentially block diagonal per simulation, in blocks corresponding to a set of quantities $(am_{ud})^2, \cdots, (aF_\pi)$. There will be large correlations within a given simulation block and smaller, respectively much smaller, ones between these blocks and the lattice spacing, respectively the renormalization constants. We then construct the fully correlated χ^2 through $\chi^2 = \sum_\beta X^T(\beta)C^{-1}(\beta)X(\beta)$, where $X(\beta)$ is the vector constructed from the difference of $y(\beta)$ and the expressions on the RHS sides of (14), appropriately repeated for each simulation. This construction guarantees that the p-value that we obtain for these fits accounts for all uncertainties and correlations.

In Fig. 1 we show a typical NLO, x-expansion fit of M_π^2 and F_π. Points with $M_\pi \gtrsim 120\,\mathrm{MeV}$ (i.e. $m_{ud} \gtrsim 3.7\,\mathrm{MeV}$) but less than $M_\pi^{\max} = 300\,\mathrm{MeV}$ (i.e. $m_{ud} \sim 23.\,\mathrm{MeV}$) are included in the combined, correlated fit. Agreement of the NLO expressions with the lattice results is excellent in this range. However the corresponding curves start deviating significantly from the lattice results for larger values of M_π.

For the NLO ξ-expansion, we perform a very similar construction. Here, however, the lattice data are $(aM_\pi)^2$, $(aM_{s\bar{s}})^2$, $2(am_{ud})/(aM_\pi)^2$, (aF_π), a, Z_A and Z_S, and the corresponding NLO expressions are:

$$\frac{2(am_{ud})}{(aM_\pi)^2} = \frac{Z_S^p}{a^p}(1+\gamma_1^a f(a^p)+\gamma_1^s(\Delta M_{s\bar{s}}^2)^p)/B_\pi^{\xi-\mathrm{NLO}}((M_\pi^2)^p;B,F,\bar{\ell}_3)\,,$$

$$(aF_\pi) \;=\; \frac{a^p}{Z_A^p}(1+\gamma_2^s(\Delta M_{s\bar{s}})^2)F_\pi^{\xi-\mathrm{NLO}}((M_\pi^2)^p;B,F,\ell_4)\,, \tag{15}$$

$$(aM_\pi)^2 = (a^p)^2(M_\pi^2)^p\,,\;\; (aM_{s\bar{s}})^2 = (a^p)^2(M_{s\bar{s}}^2)^p\,, \tag{16}$$

$$a = a^p\,,\;\; Z_A = Z_A^p\,,\;\; Z_S = Z_S^p,$$

where $1/B_\pi^{\xi-\mathrm{NLO}}((M_\pi^2)^p;B,F,\bar{\ell}_3)$ is $1/B$ times the NLO part of the expression in brackets on the RHS of the first equation in (7). $F_\pi^{\xi-\mathrm{NLO}}((M_\pi^2)^p;B,F,\ell_4)$ is the expression obtained by solving exactly the NLO part of the second equation in (7) for F_π, and keeping the physical solution. This equation is quadratic in F_π and the existence of a physical solution is not guaranteed. The existence of such a solution imposes a constraint on the LO and NLO $SU(2)$ χPT parameters, which we take into account in our fits. We discuss these solutions and constraints in more detail in Appendix A.

We show typical NLO ξ-expansion fits in Fig. 2. Again, only points with M_π less than $M_\pi^{\max} = 300\,\mathrm{MeV}$ are included. The behavior found here is quite similar to the one found above for the NLO x-expansion, with the fit curves agreeing well with the lattice results in the fit range, but deviating more and more beyond that. However, the deviations beyond $M_\pi^{\max} = 300\,\mathrm{MeV}$ are slightly less pronounced than in the x-expansion. This is probably a demonstration of the statement made in the Introduction, that the ξ-expansion resums some higher-order physical contributions.

We now turn to NNLO fits. The procedure followed here is identical to the one described above for NLO fits, except that the NLO expressions in Eqs. (14)–(15) are replaced by the appropriate NNLO expressions from Sec. 1. That is $B_\pi^{x-\mathrm{NLO}}(m_{ud}^p;B,F,\bar{\ell}_3)$, $F_\pi^{x-\mathrm{NLO}}(m_{ud}^p;B,F,\bar{\ell}_4)$, $B_\pi^{\xi-\mathrm{NLO}}((M_\pi^2)^p;B,F,\bar{\ell}_3)$ and $F_\pi^{\xi-\mathrm{NLO}}((M_\pi^2)^p;B,F,\bar{\ell}_4)$ are replaced by $B_\pi^{x-\mathrm{NNLO}}(m_{ud}^p;B,F,\bar{\ell}_3,\bar{\ell}_{12},k_M)$, $F_\pi^{x-\mathrm{NNLO}}(m_{ud}^p;B,F,\bar{\ell}_4,\bar{\ell}_{12},k_F)$, $B_\pi^{\xi-\mathrm{NNLO}}((M_\pi^2)^p;B,F,\bar{\ell}_3,\bar{\ell}_{12},c_M)$ and $F_\pi^{\xi-\mathrm{NNLO}}((M_\pi^2)^p;B,F,\bar{\ell}_4,\bar{\ell}_{12},c_F)$. Thus, in addition to the 4 χPT parameters required in the NLO fits, the NNLO expressions contain 5 additional chiral parameters: $\bar{\ell}_{12}$, k_M and k_F for the x-expansion and $\bar{\ell}_{12}$, c_M and c_F for the ξ-expansion.

$F_\pi^{\xi-\mathrm{NNLO}}((M_\pi^2)^p;B,F,\bar{\ell}_4,\bar{\ell}_{12},c_F)$ is the expression obtained by solving exactly the quartic, second equation in (7) for F_π, and by keeping the physical solution. Again, the existence of a physical solution imposes constraints on the LO, NLO and now NNLO $SU(2)$ χPT parameters. We take these constraint into account in our fits. In Appendix A we give the physical solution and discuss the conditions for its existence in more detail.

Defining the χ^2 as we do for the NLO fits, we perform fully correlated, NNLO x and ξ-expansion fits to M_π^2 and F_π, with $M_\pi^{\max}$ between 400 and 550 MeV. A typical example of such a fit is shown in Fig. 3 for the x-expansion, and in Fig. 4 for the ξ-expansion, both for $M_\pi^{\max} = 500\,\mathrm{MeV}$. The p-values of these fits are excellent. The agreement with the lattice results is also visibly very good and extends better beyond $M_\pi^{\max}$ than in the NLO case. In both the x and ξ-expansions, the NNLO serves to cancel the curvature of the NLO forms to give a more linear behavior of the mass dependence of M_π^2 and F_π.

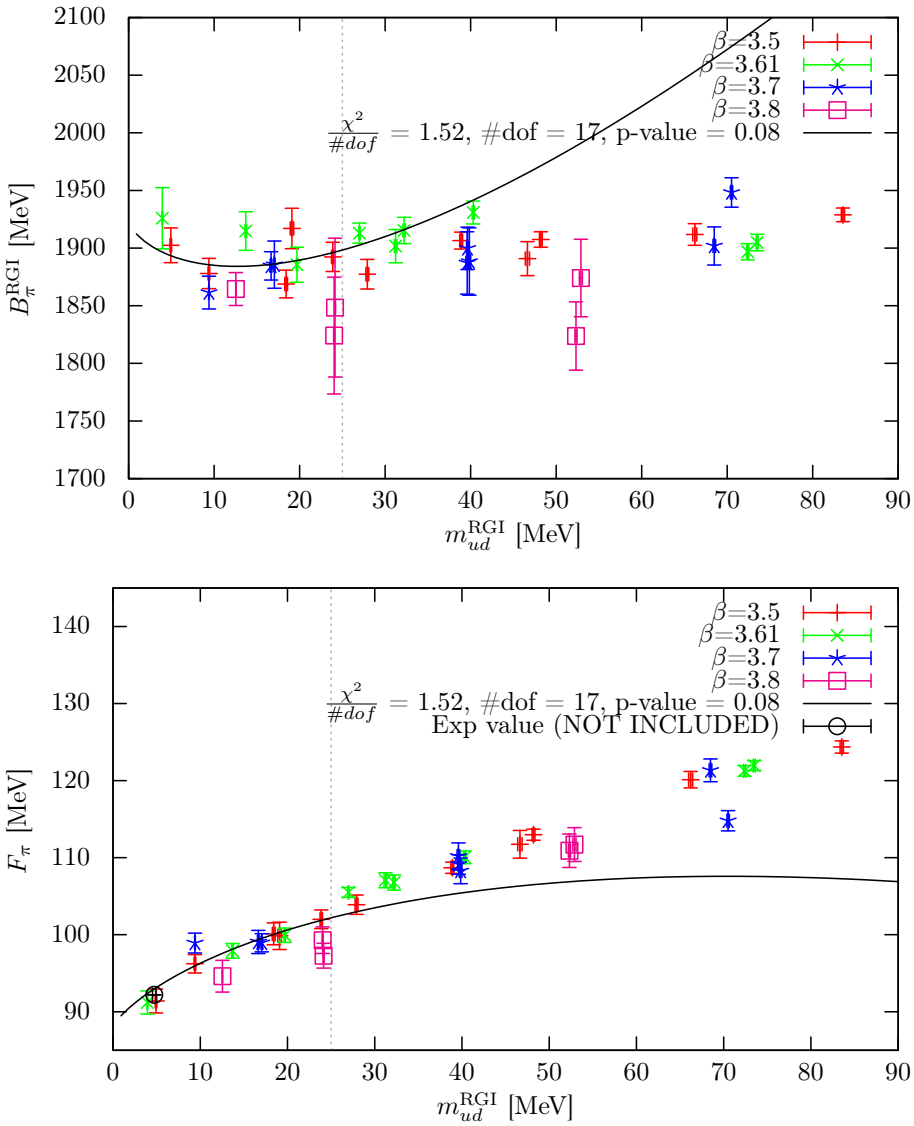

Figure 1: *Typical NLO $SU(2)$ χPT fit (curves) of our lattice results (points with error bars) for $B_\pi = M_\pi^2/(2m_{ud})$ and F_π as functions of m_{ud}, in the x-expansion. These are fully correlated fits to the NLO expressions of (14), which also account for discretization and strange quark mass corrections. Only points with $M_\pi \leq M_\pi^{\max} = 300\,\mathrm{MeV}$ (i.e. $m_{ud} \sim 23.\,\mathrm{MeV}$) are included in the fits, i.e. those left of the dashed vertical line. The more massive points are shown for illustration. The lattice results in the figure are corrected for discretization and strange mass contributions, using the fit parameters obtained. Thus, they are continuum limit results at the physical value of m_s and their only residual dependence is on m_{ud}. Nevertheless, results obtained at different lattice spacing are plotted with different symbols. The fact that they lie on a same curve indicates that residual discretization errors are negligible. Note that the corrections made to the more massive points may not be optimal as these points are not included in the fit and, as we will see, the applicability of NLO χPT is questionable for these points. Error bars on all points are statistical only. Also shown, but not included in the fits, is the experimental value of F_π [46]. Agreement with our results computed directly around the physical pion mass point is remarkable.*

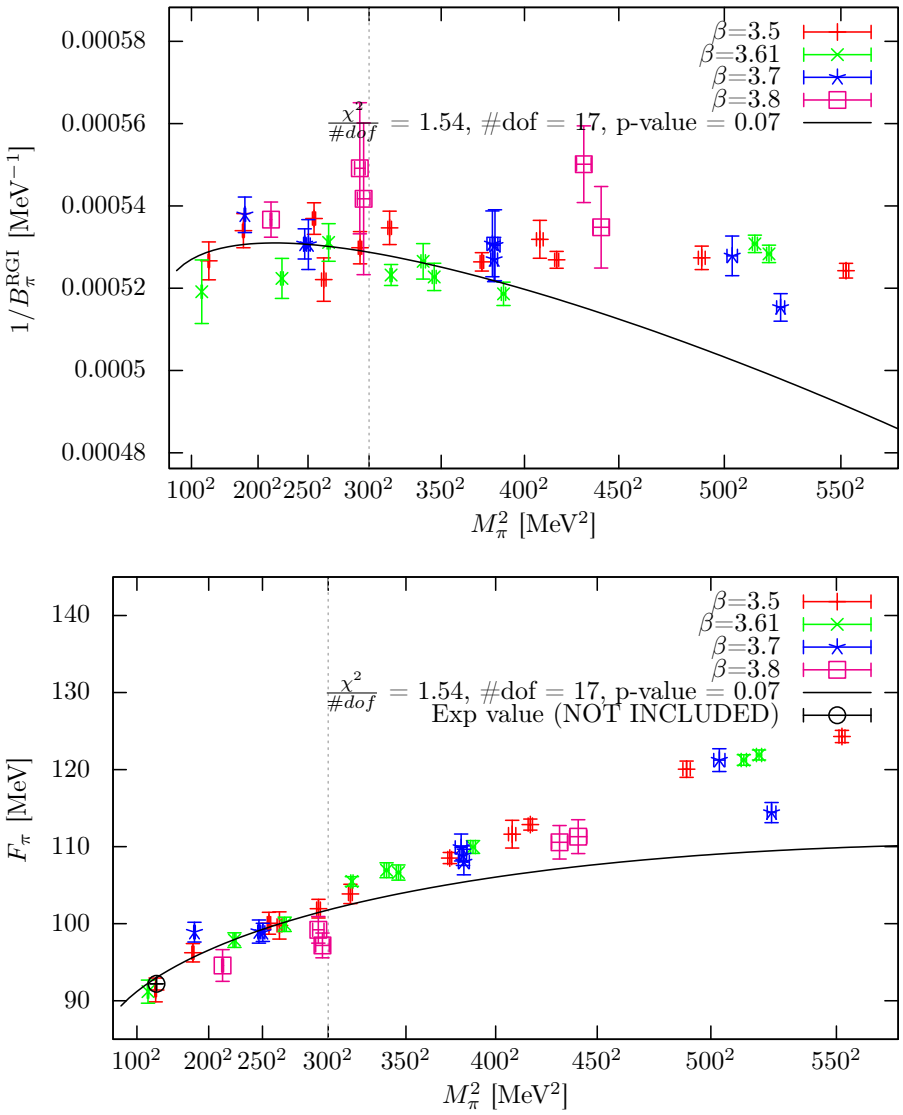

Figure 2: *Typical NLO $SU(2)$ χPT fit (curves) of our lattice results (points with error bars) for $1/B_\pi$ and F_π as functions of M_π^2, in the ξ-expansion. Only points with $M_\pi \leq M_\pi^{\max} = 300\,\mathrm{MeV}$ are included in the fits, i.e. those left of the dashed vertical line. The description is the same as in Fig. 1, except that the functional forms used are those of (15).*

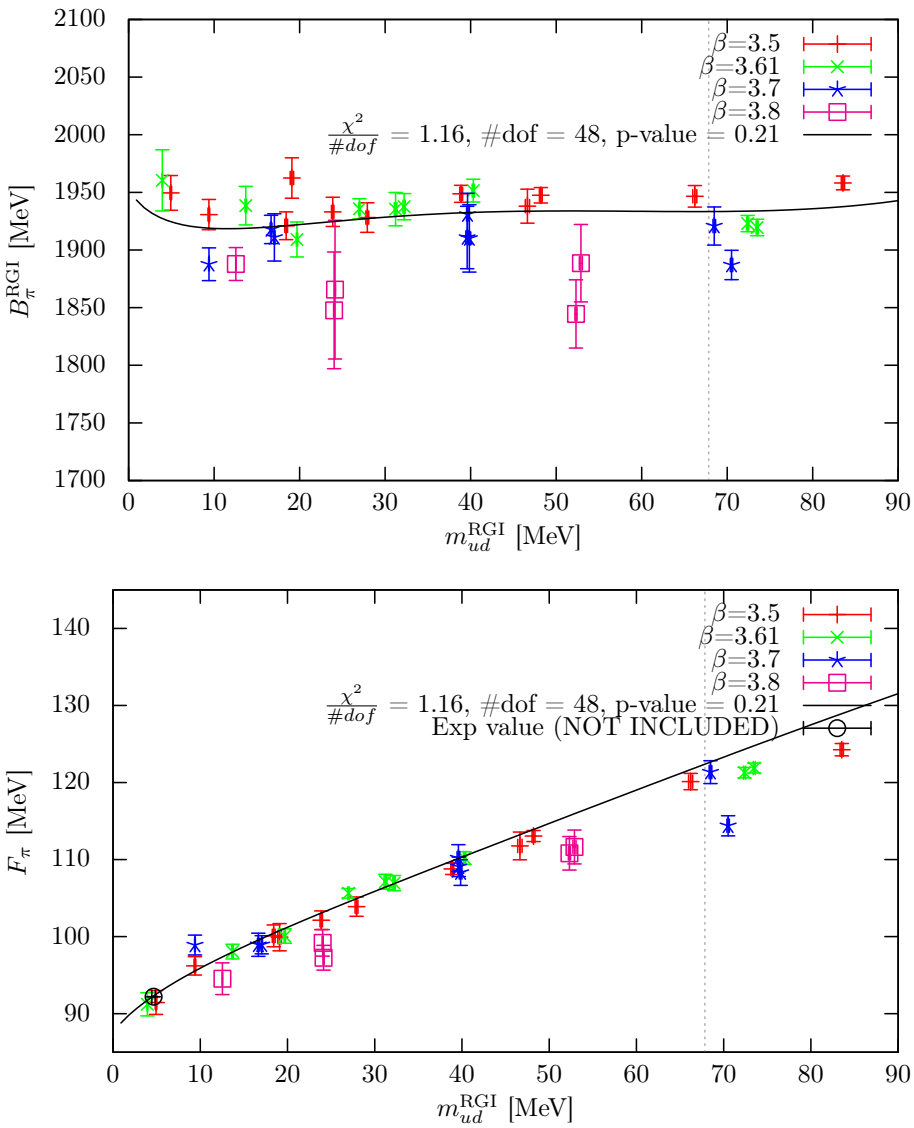

Figure 3: *Typical NNLO $SU(2)$ χPT fit (curves) of our lattice results (points with error bars) for B_π and F_π as functions of m_{ud}, in the x-expansion. Only points with $M_\pi \leq M_\pi^{\max} = 500\,\mathrm{MeV}$ (i.e. $m_{ud}^{\max} \lesssim 65.\,\mathrm{MeV}$) are included in the fits, i.e. those left of the dashed vertical line. The description is the same as in Fig. 1, except that the functional forms used are those of (14) with B_π^{x-NLO} and F_π^{x-NLO} replaced by B_π^{x-NNLO} and F_π^{x-NNLO}, respectively.*

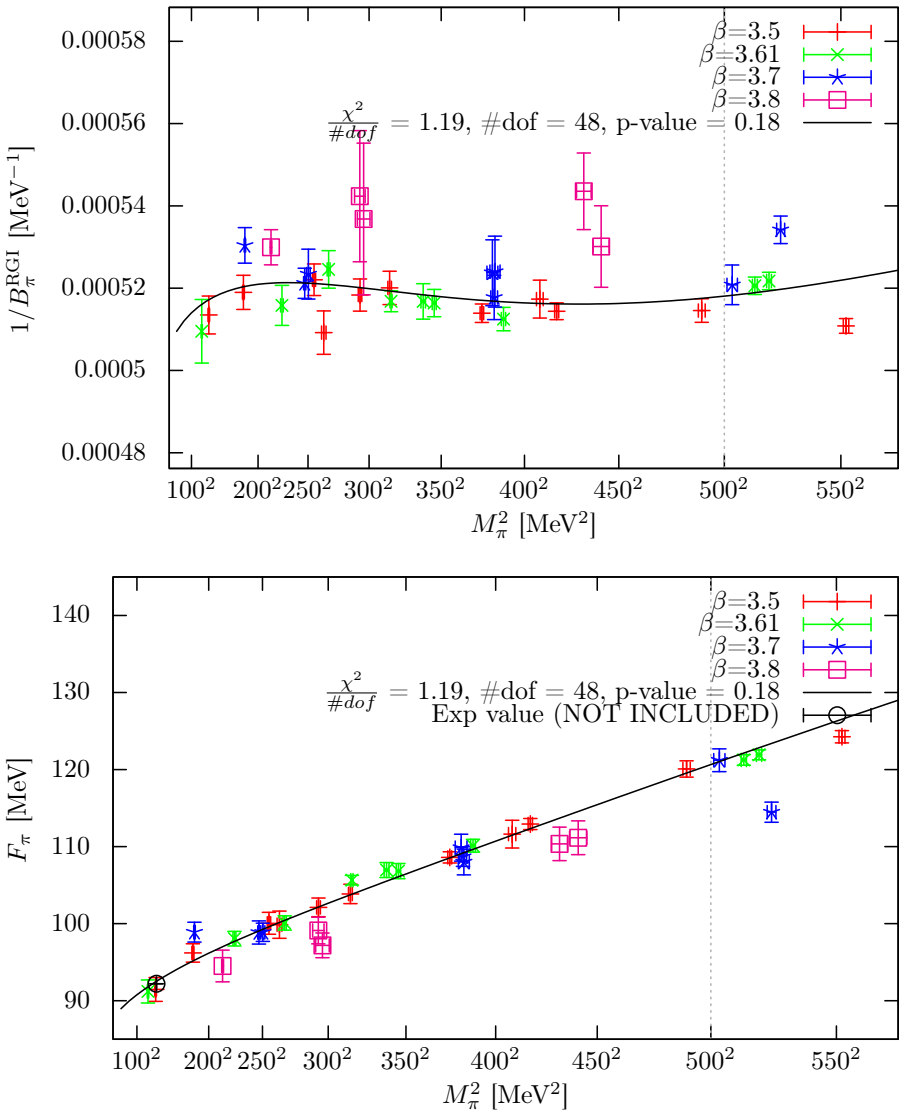

Figure 4: *Typical NNLO $SU(2)$ χPT fit (curves) of our lattice results (points with error bars) for $1/B_\pi$ and F_π as functions of M_π^2, in the ξ-expansion. Only points with $M_\pi \leq M_\pi^{\rm max} = 500\,{\rm MeV}$ are included in the fits, i.e. those left of the dashed vertical line. The description is the same as in Fig. 1, except that the function forms used are those of (15) with $B_\pi^{\xi-{\rm NLO}}$ and $F_\pi^{\xi-{\rm NLO}}$ replaced by $B_\pi^{\xi-{\rm NNLO}}$ and $F_\pi^{\xi-{\rm NNLO}}$, respectively.*

3.2 Fit quality and LECs in terms of maximum pion mass for NLO χPT

We now turn to our systematic study of the range of applicability of $SU(2)$ chiral perturbation theory to the quark-mass dependence of M_π^2 and F_π. We implement the fully correlated, combined fits described above, including lattice results extending from our smallest pion mass of around 120 MeV up to a maximal value, $M_\pi^{\max}$. We then study the p-value of these fits as a function of $M_\pi^{\max}$. We consider NLO x and ξ-expansion fits in this section and NNLO ones in the following. For the x-expansion fits, the cut is made at a value of m_{ud} corresponding to $M_\pi^{\max}$ such that the same lattice results are include as would be with a cut at $M_\pi^{\max}$ in the ξ-expansion fits.

For each value of $M_\pi^{\max}$ and for each functional form tried, we compute the fit quality, including a systematic error. Indeed, we want to make sure that the p-value which we quote is not peculiar to a particular choice of analysis procedure. This is particularly important in fits, such as those performed here, where the observables considered have significant correlations and small changes can make large changes in the fit quality. The p-values are obtained from the p-value-weighted distributions of results from $2 \times 2 \times 3 \times 6 = 72$ different analysis procedures for a given $M_\pi^{\max}$. These procedures correspond to 2 time-fit intervals for the two-point functions, 2 mass cuts in the scale setting, 3 ways of doing RI/MOM renormalization for Z_A and 6 for Z_S, as described in Sec. 2. The central value of the fit quality for a given $M_\pi^{\max}$ is chosen as the mean of the corresponding distribution and its systematic error obtained from this distribution's variance.

The results for the the p-values of our NLO and NNLO, x and ξ-expansion fits are shown together in Fig. 5. For the NLO fits we consider values of $M_\pi^{\max}$ between 250 and 450 MeV. Below 250 MeV the number of lattice points which we have starts becoming too small to reliably constrain the NLO form. Above 450 MeV, these fits have tiny p-values.

As Fig. 5 shows, the NLO x and ξ-expansion fits work very well for $M_\pi^{\max} \leq 300\,\text{MeV}$. There is a first drop in p-value for $M_\pi^{\max}$ in the region of 350 to 400 MeV in which fit qualities are in the 1 to 10% range. Between 400 and 450 MeV the fit quality drops enormously and keeps on doing so beyond that point (not shown). We have checked that these changes are not the artefact of a single stray point in these intervals. This discussion suggests that, for M_π^2 and F_π, the range of validity of $SU(2)$ extends safely up to 300 MeV and may be stretched up to around 400 MeV. Beyond that point it clearly breaks down. Of course, these conclusions only hold within the statistical accuracy of our calculation, which is described in more detail in Sec. 3.4.

It is worth noting that the break-down is less pronounced for the NLO ξ-expansion. This may be ascribed in part to a difference in size in the relative uncertainties on M_π^2 and m_{ud}. It also seems to corroborate the observation, made in Sec. 3.1, that the ξ-expansion range of applicability may extend to slightly larger quark-mass values because it resums some higher-order physical contributions.

In order to further verify the conclusions drawn up to now, we also monitor the values of the fitted LECs, as a function of $M_\pi^{\max}$. We begin with the LO LECs B and F. Their values as a function of $M_\pi^{\max}$ are shown in Fig. 6 for the NLO x and ξ-expansions. These values include full statistical and systematic errors, obtained with the same collection of analyses as those used in determining the p-values. For each quantity, we weigh the result given in each procedure by its p-value. This yields a distribution of results for each quantity. The central value for each quantity is chosen to be the mean of the distributions. Its systematic uncertainty is obtained by computing the variance with respect to the mean, over this distribution.

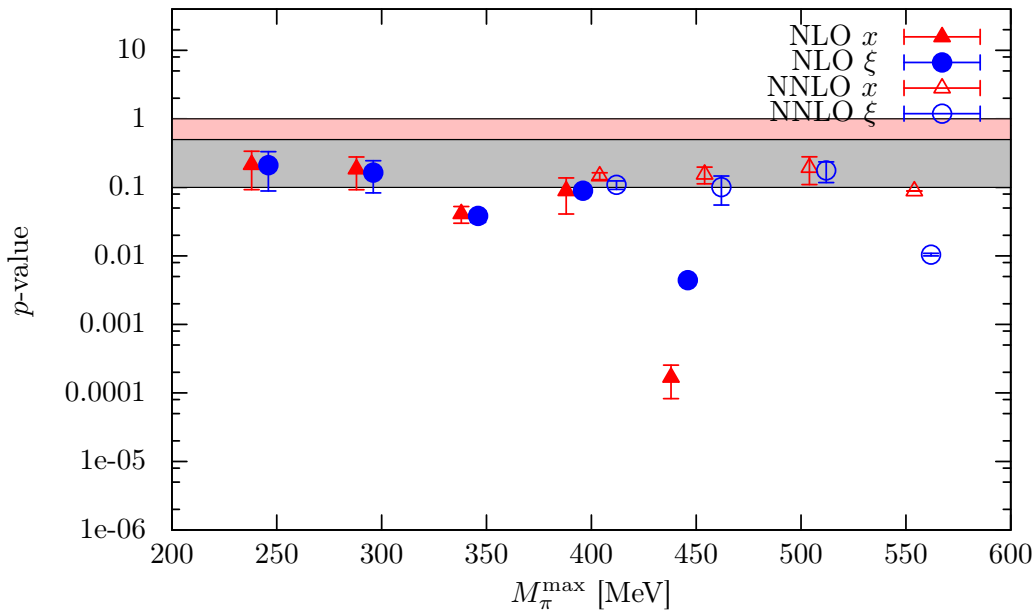

Figure 5: *Fit quality of the fully correlated $SU(2)$ χPT fits to our lattice results for B_π and F_π described in Sec. 3.1. The fits to our lattice results for these quantities include points whose pion mass is in the range $[120\,\text{MeV}, M_\pi^{\max}]$. The p-values shown are those of NLO and NNLO fits in the x and ξ-expansions. They are are plotted as a function of $M_\pi^{\max}$. For $M_\pi^{\max} \leq 350\,\text{MeV}$, only the p-values of NLO fits are plotted as these ranges do not contain enough data to constrain NNLO chiral expressions. For $M_\pi^{\max} \in [400, 450]\,\text{MeV}$, the p-values of both NLO and NNLO fits are shown. For larger $M_\pi^{\max}$ only NNLO results are shown, as the p-values of NLO fits are negligibly small. The gray band corresponds to the p-value interval of 10 to 50% and the red one to that of 50 to 100%. Error bars on each point are the systematic uncertainties described in the text. For the sake of clarity, results are shifted about the values of $M_\pi^{\max} = 250, \cdots$ MeV, at which they are obtained.*

Finally, the statistical error is obtained by repeating the construction of the distributions for the 2000 bootstrap samples, and considering the variance of these means around the central value.

As the plots show, the LO LECs obtained from NLO fits jump for $M_\pi^{\max}$ between 300 and 350 MeV, but appear to remain consistent within errors. However, because the values of the LECs for two different pion mass cuts are obtained from data sets which have significant overlap, they are correlated, which may give a false impression of agreement. In order to eliminate the effect of these correlations in the comparison, we study the quantities ΔB^{RGI} and ΔF, which are the differences of the LECs at the given value of $M_\pi^{\max}$ minus the ones obtained for $M_\pi^{\max} = 300\,\text{MeV}$. The latter is chosen because it is clearly within the range of applicability of $SU(2)$ χPT, at the level of accuracy considered here. We compute the statistical and systematic errors directly on these differences, both within our bootstrap resampling and systematic error analysis loops. The errors on these differences determine directly the significance of the deviations of the values of the LECs obtained for a given $M_\pi^{\max}$ with that obtained for $M_\pi^{\max} = 300\,\text{MeV}$. These differences are plotted in Fig. 6, in a panel below the

corresponding LEC. By definition, $\Delta B^{\rm RGI}$ and ΔF are exactly zero at $M_\pi^{\rm max} = 300\,{\rm MeV}$.

The plots of these differences show that the seeming agreement deduced from a direct comparison of the values of the LECs at two different pion mass cuts is misleading. While one finds that the values of the LO LECs for $M_\pi^{\rm max} = 250$ and 300 MeV agree within one standard deviation, this is no longer true for values of $M_\pi^{\rm max} \geq 350\,{\rm MeV}$. Indeed, the values of $\Delta B^{\rm RGI}$ and ΔF are almost 2 standard deviations away from 0 and more for $M_\pi^{\rm max} = 400\,{\rm MeV}$. Beyond that point, the values of the LECs obtained from NLO fits are not meaningful, because the quality of the fits becomes so poor. The results on these differences sharpen the earlier conclusion that NLO, $SU(2)$ χPT starts breaking down above 300 MeV, for the precisions reached here.

We perform a very similar analysis for the NLO LECs, $\bar{\ell}_3$ and $\bar{\ell}_4$, extracted from our combined, correlated NLO fits. In particular, we define the differences $\Delta\bar{\ell}_3$ and $\Delta\bar{\ell}_4$ in full analogy with $\Delta B^{\rm RGI}$ and ΔF. These LECs and their differences with respect to their values for $M_\pi^{\rm max} = 300\,{\rm MeV}$ are plotted as a function of $M_\pi^{\rm max}$ in Fig. 7. The jump between $M_\pi^{\rm max} = 300$ and 350 MeV observed in the p-values and in $\Delta B^{\rm RGI}$ and ΔF is still present in $\Delta\bar{\ell}_4$, but less so in $\Delta\bar{\ell}_3$. It is also interesting to note that for $M_\pi^{\rm max} \geq 350\,{\rm MeV}$, the values of $\bar{\ell}_4$ obtained from the x and ξ-expansion fits are no longer compatible, a clear sign that higher order contributions are becoming relevant. Thus these NLO LEC results are compatible with the conclusions drawn so far as to the range of applicability of NLO, $SU(2)$ χPT.

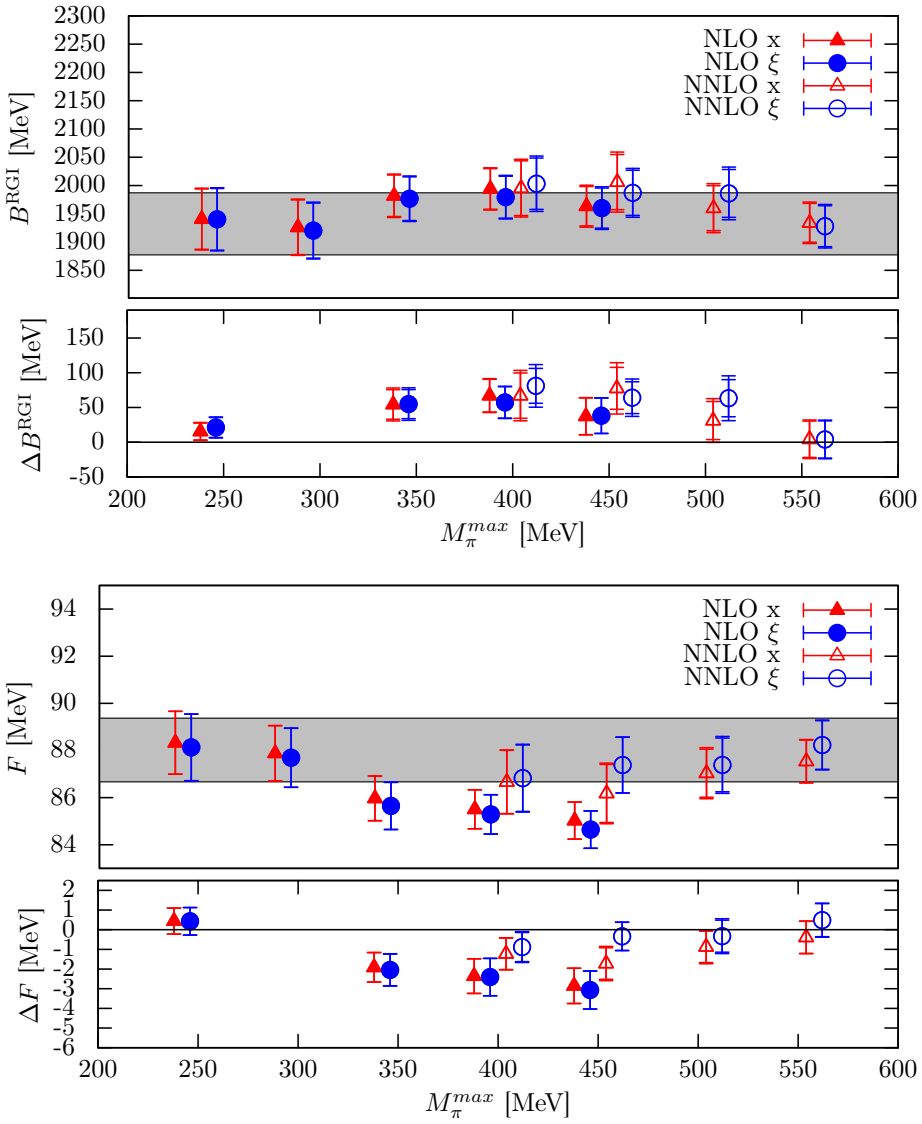

Figure 6: *LO LECs as a function of* $M_\pi^{\rm max}$ *obtained from the* $SU(2)$ χPT *fits to our lattice results for* B_π *and* F_π *in the pion-mass range* $[120\,\text{MeV},\, M_\pi^{\rm max}]$*, as described in Sec. 3.1. Results are shown for NLO and NNLO fits in the* x *and* ξ*-expansions (see the caption of Fig. 5 for additional details). In the top panel of each of the two figures, it is the LEC in physical units which is shown. The horizontal gray band denotes our final result for the corresponding LEC, given in Table 4, and obtained as described in Sec. 4. In the lower panel of each figure it is the difference of the LEC obtained from a fit with* $M_\pi \in [120\,\text{MeV},\, M_\pi^{\rm max}]$ *to that obtained from the NLO fit in the range* $[120,\, 300]\,\text{MeV}$*, in the corresponding expansion. As argued in the text, this reference domain is in the range of applicability of NLO* χPT *at our level of accuracy. Error bars on each point are the statistical and the quadratically combined statistical-plus-systematic uncertainties. For the sake of clarity, results are shifted about the values of* $M_\pi^{\rm max} = 250, \cdots$ MeV*, at which they are obtained.*

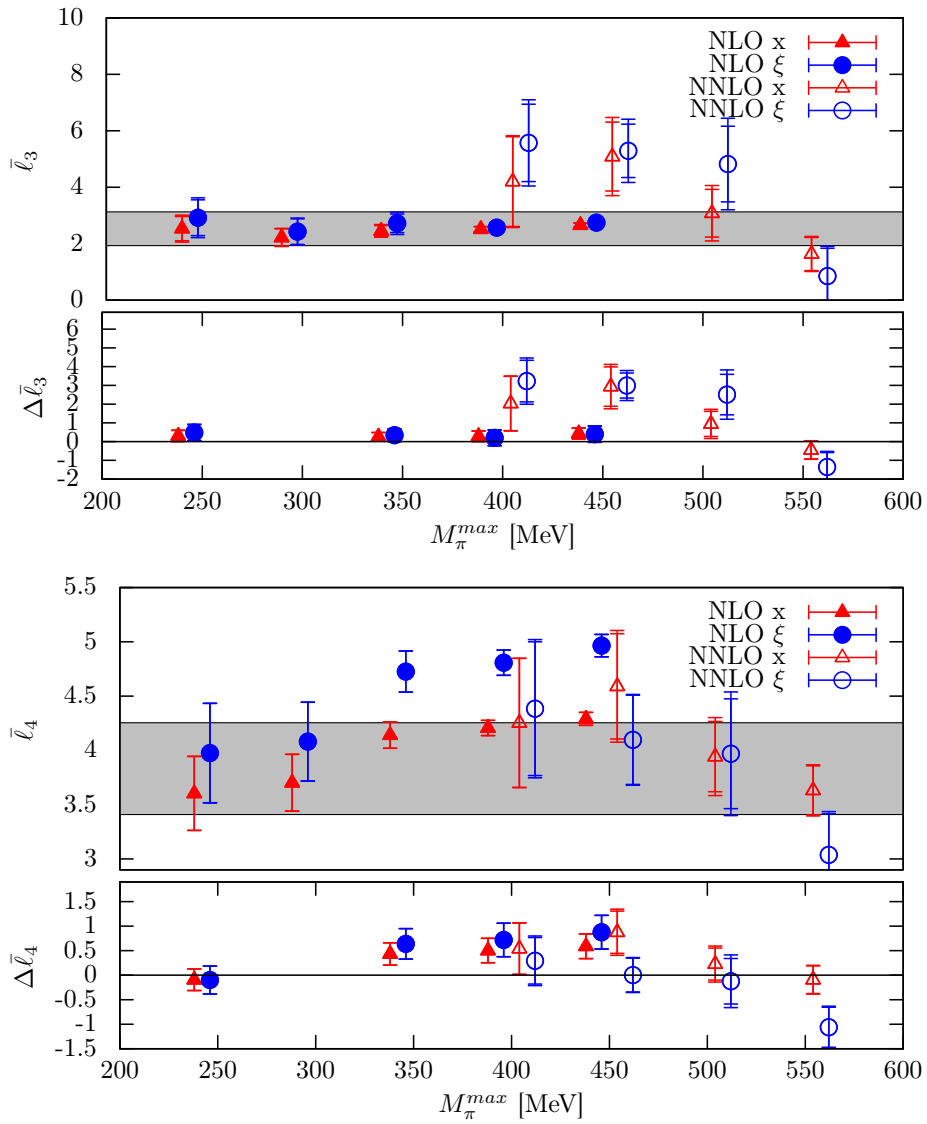

Figure 7: *NLO LECs as a function of* $M_\pi^{\max}$ *obtained from the* $SU(2)$ χPT *fits to our lattice results for* B_π *and* F_π *in the pion mass range* $[120\,\text{MeV},\, M_\pi^{\max}]$*, as described in Sec. 3.1. This figure is the same as Fig. 6, but for NLO instead of LO LECs.*

3.3 Fit quality and LECs in terms of maximum pion mass for NNLO χPT

We now turn to the study of NNLO $SU(2)$ χPT. The analysis we perform here parallels the one discussed above for NLO χPT. In particular, we study the dependence of the p-value and the LECs as a function of $M_\pi^{\max}$. Here there are 5 additional LECs that have to be considered. These are $\bar{\ell}_{12}$, k_M and k_F, in the case of the x-expansion, and $\bar{\ell}_{12}$, c_M and c_F for the ξ-expansion. The lowest value of $M_\pi^{\max}$ that we consider is 400 MeV, because NLO fits work reasonably well up to around that point and because we need more lever-arm and data to fix the 3 additional parameters required at NNLO in each expansion.

The results for the fit quality as a function of $M_\pi^{\max}$ are shown in Fig. 5, together with the results from NLO fits. As these show, the introduction of NNLO terms brings the p-values back up to acceptable values up to $M_\pi^{\max} \simeq 500\,\text{MeV}$. Beyond that point the p-values of NNLO fits also drop. These observations suggest that the NNLO, $SU(2)$ chiral expansion of M_π^2 and F_π may extend up to 500 MeV, at least for the statistical precision reached in this work and described in Sec. 3.4.

To check this statement, we turn to the study of the LECs as a function of $M_\pi^{\max}$. The results for the LO LECs, B^{RGI} and F, are show in Fig. 6 and those for the NLO LECs, $\bar{\ell}_3$ and $\bar{\ell}_4$, are given in Fig. 7, together with the results obtained from the NLO fits discussed in the previous section.

The results for F and $\bar{\ell}_4$ appear to confirm the conclusions drawn from the behavior of the p-values, at least for the ξ-expansion. In that case, the addition of NNLO terms for $M_\pi^{\max} \geq 400\,\text{MeV}$ brings the values of F and $\bar{\ell}_4$, associated with F_π, back in line with those obtained at NLO, with $M_\pi^{\max} = 300\,\text{MeV}$. This suggests that the NNLO terms are just what is needed to accommodate the tensions which appear in the NLO fits for $M_\pi^{\max} \gtrsim 350\,\text{MeV}$. However this picture is not fully borne out by the LECs associated with the quark-mass dependence of M_π^2. Indeed the jump in B^{RGI}, observed in NLO fits in the region of pion-mass cuts between 300 and 350 MeV, remains present for $M_\pi^{\max} \sim 400$ to 450 MeV, despite the addition of NNLO terms. Similar features are observed in the x-expansion, though the addition of NNLO terms reduces the jump in F and $\bar{\ell}_4$ less than it does in the ξ-expansion.

In view of this discussion, we conclude that the addition of NNLO terms appears to allow a description of the mass dependence of F_π up to a pion mass of around 500 MeV, which is consistent with NLO fits in a smaller range of pion masses. This is more true for the expansion in ξ than it is for the one in x. However, this apparent extension of the applicability range does not carry over to the study of the chiral behavior of B_π, suggesting that the NNLO chiral expansion of this quantity begins to fail for $M_\pi^{\max}$ in the region of 300 to 350 MeV, for the accuracies reached here. Moreover, it is important to remember that B_π and F_π share common LECs and lattice data, and are fitted together. Thus, there is limited sense in suggesting that the range of applicability of χPT for these two quantities differs.

For completeness, in Fig. 8 we show results for the NNLO x-expansion LECs, k_M and k_F, as well as results for the NNLO ξ-expansion LECs, c_M and c_F, as functions of $M_\pi^{\max}$. At NNLO these fits also allow the determination of the linear combination of the NLO LECs $\bar{\ell}_1$ and $\bar{\ell}_2$ given by $\bar{\ell}_{12}$ that is defined after Eq. (4). This combination is also shown in Fig. 8 as a function of $M_\pi^{\max}$. The uncertainties on all of these coefficients are large, since the precision of our results is barely sufficient to determine these higher order contributions, at least for $M_\pi^{\max} \leq 450\,\text{MeV}$. The coefficients k_M and k_F of the x-expansion show little dependence on $M_\pi^{\max}$ all he way up to 550 MeV. This is only the case up to 500 MeV for k_M and k_F of the ξ-expansion. In both expansions, $\bar{\ell}_{12}$ drop beyond $M_\pi^{\max} = 500\,\text{MeV}$. However, it is worth

noting that the x-expansion gives a value of $\bar{\ell}_{12}$ which is consistent with the determination of [12] discussed below in Sec. 4, for $M_\pi^{\max} \leq 500\,\mathrm{MeV}$. The ξ-expansion yields values which are larger.

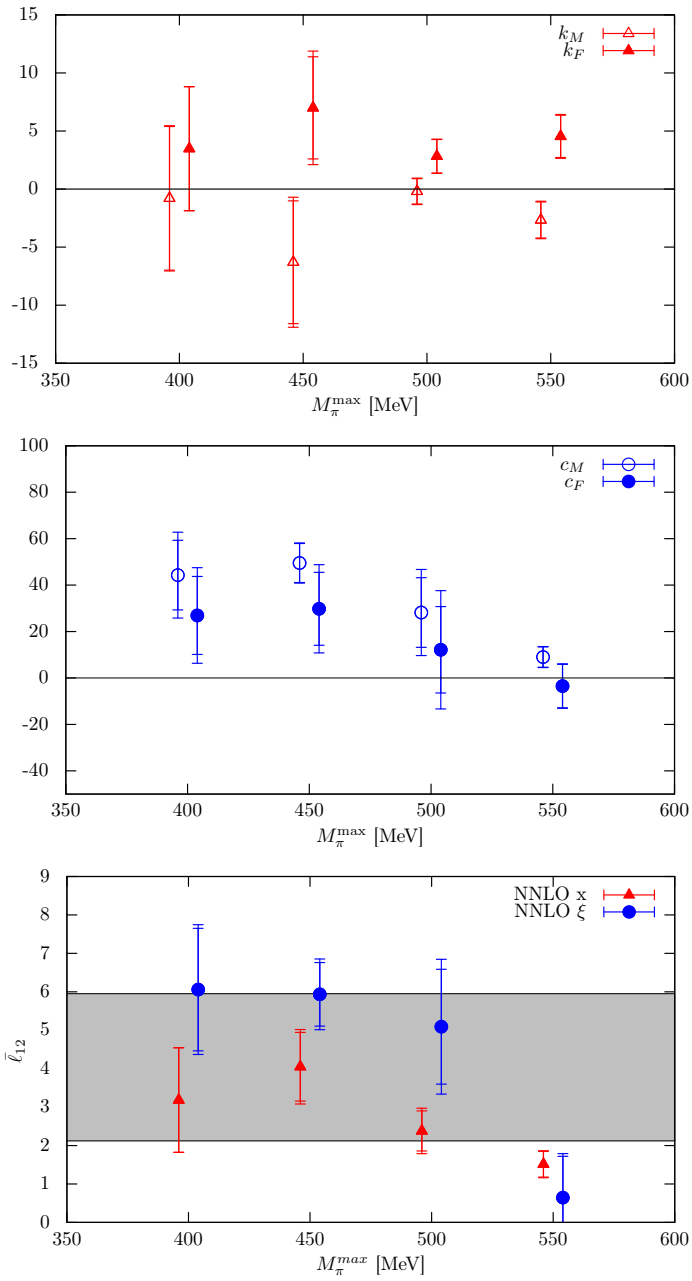

Figure 8: *LECs which appear at NNLO in the $SU(2)$ χPT expansions of B_π and F_π given in Eqs. (2)–(7). The top figure shows the results obtained for k_M and k_F from NNLO fits in the x-expansion to our lattice results with $M_\pi \in [120\,\text{MeV}, M_\pi^{\max}]$. The results are plotted as functions of $M_\pi^{\max}$. In the middle figure are plotted the NNLO LECs c_M and c_F, which appear in the ξ-expansion. The NLO LEC combination $\bar{\ell}_{12} = (7\bar{\ell}_1 + 8\bar{\ell}_2)/15$ appears in the the x and ξ-expansions of B_π and F_π at NNLO. The results that we obtain for this LEC in each of the expansions are plotted in the bottom panel. The horizontal gray band denotes our final result for $\bar{\ell}_{12}$, obtained as described in Sec. 4. Error bars on each point are the statistical and the quadratically combined statistical-plus-systematic uncertainties. For the sake of clarity, results are shifted about the values of $M_\pi^{\max} = 250, \cdots$ MeV, at which they are obtained.*

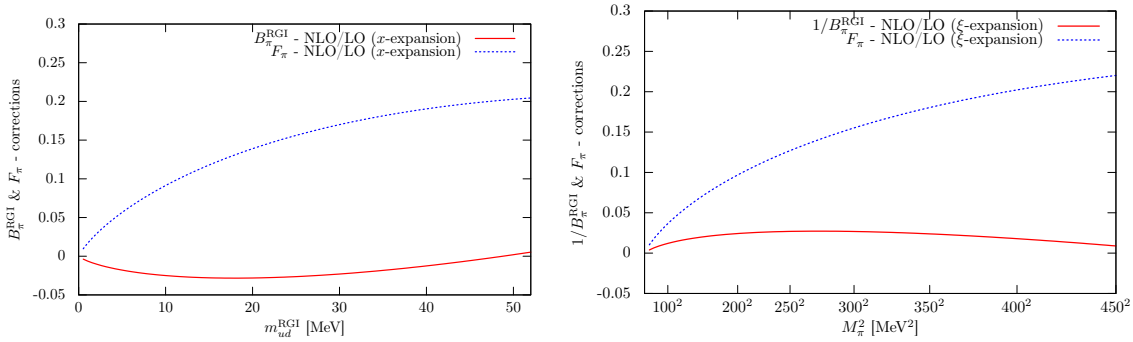

Figure 9: *Ratios of the NLO contributions to B_π and F_π with respect to the LO ones, as a function of m_{ud} in the $SU(2)$ chiral x-expansion (left panel) and of M_π^2, in the ξ-expansion (right panel). The values of the LECs used are those given in Table 3 for the respective expansions.*

3.4 Relative contributions of different orders in χPT and conclusions on its range of applicability

As a final indication on the range of applicability of $SU(2)$ χPT to B_π and F_π, we consider the size of NLO and NNLO contributions relative to the LO ones, as functions of m_{ud} and M_π^2. We do so for two purposes. The first is to verify that the corrections obtained in the NLO fits, which we perform for $M_\pi^{\rm max} \leq 400\,{\rm MeV}$ (i.e. $(m_{ud}^{\rm RGI})^{\rm max} \leq 41.\,{\rm MeV}$), remain reasonable over the mass range $M_\pi \in [120\,{\rm MeV}, M_\pi^{\rm max}]$ (i.e. $m_{ud}^{\rm RGI} \in [3.7\,{\rm MeV}, (m_{ud}^{\rm RGI})^{\rm max}]$). The second reason for investigating the size of these corrections is to further assess the validity of our NNLO fits which include points up to $M_\pi^{\rm max} \simeq 500\,{\rm MeV}$ (i.e. $(m_{ud}^{\rm RGI})^{\rm max} \simeq 65\,{\rm MeV}$).

In Fig. 9 we plot together the NLO corrections to B_π and F_π in the x-expansion with those of $1/B_\pi$ and F_π in the ξ-expansion, for $m_{ud}^{\rm RGI} \leq 52.\,{\rm MeV}$, respectively $M_\pi \leq 450\,{\rm MeV}$. As the plots show, the NLO corrections on F_π remain less than about 10% for $M_\pi \leq 200\,{\rm MeV}$ (i.e. $m_{ud}^{\rm RGI} \leq 10.\,{\rm MeV}$), less than about 15% for $M_\pi \leq 300\,{\rm MeV}$ (i.e. $m_{ud}^{\rm RGI} \leq 23.\,{\rm MeV}$) and less than about 20% for $M_\pi \leq 400\,{\rm MeV}$ (i.e. $m_{ud}^{\rm RGI} \leq 41.\,{\rm MeV}$). The NLO corrections on B_π are significantly smaller. They remain significantly less than 5% all the way up to $M_\pi = 450\,{\rm MeV}$ (i.e. $m_{ud}^{\rm RGI} \leq 52.\,{\rm MeV}$). However they exhibit non-monotonic behavior, with a turnover around $M_\pi \sim 280\,{\rm MeV}$ (i.e. $m_{ud}^{\rm RGI} \sim 20.\,{\rm MeV}$). All of this is entirely consistent with the picture, drawn earlier, that our results with errors on the order of a percent start becoming sensitive to NNLO effects for $M_\pi \sim 300\,{\rm MeV}$ and require their presence beyond $M_\pi \gtrsim 400\,{\rm MeV}$.

Now let us investigate the size of the NLO and NNLO corrections in our NNLO fits. For this we consider the same typical NNLO fits that were shown in Fig. 3 for the x-expansion and Fig. 4 for the ξ-expansion. We plot the relative size of the NLO and NNLO corrections to B_π and F_π as a function of $m_{ud}^{\rm RGI}$ in Fig. 10 for the x-expansion and in Fig. 11 as a function of M_π^2 for the ξ-expansion. Although the p-values of our NNLO fits remain good up to $M_\pi \sim 500\,{\rm MeV}$ (i.e. $m_{ud}^{\rm RGI} \sim 65.\,{\rm MeV}$), at that value of M_π the NNLO corrections to F_π are a significant fraction of the NLO corrections, raising doubts as to the legitimacy of neglecting NNNLO terms in these fits. This is more than confirmed by the corrections to B_π for which the NNLO corrections are already a significant fraction of the NLO corrections for $M_\pi \sim 300\,{\rm MeV}$ or $m_{ud}^{\rm RGI} \sim 23.\,{\rm MeV}$. Moreover, these NLO and NNLO corrections have here

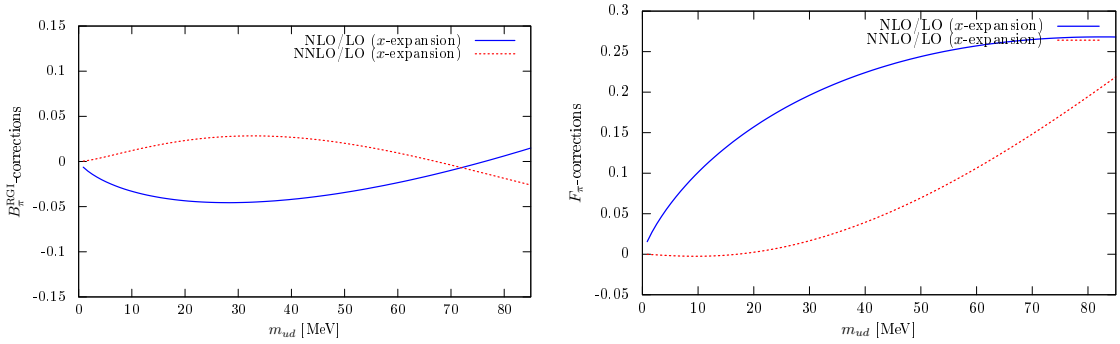

Figure 10: *Typical ratios of the NLO and NNLO contributions to B_π (left panel) and F_π (right panel) with respect to the LO ones, as a function of m_{ud} in the $SU(2)$ chiral x-expansion. The values of the LECs used are those obtained from the fit shown in Fig. 3.*

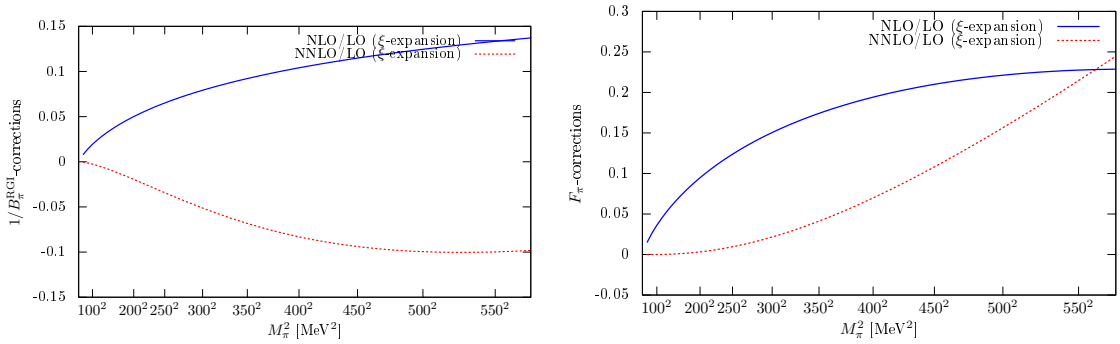

Figure 11: *Typical ratios of the NLO and NNLO contributions to $1/B_\pi$ (left panel) and F_π (right panel) with respect to the LO ones, as a function of M_π^2 in the $SU(2)$ chiral ξ-expansion. The values of the LECs used are those obtained from the fit shown in Fig. 4.*

opposite signs, implying cancellations which may be affected by the inclusion of higher-order terms at larger pion-mass values.

It is worth noting that the expansion appears better behaved for F_π than for B_π, since the hierarchy of corrections for the former remains acceptable up to $M_\pi \sim 450\,\text{MeV}$ or $m_{ud}^{\rm RGI} \sim 52.\,\text{MeV}$. The situation is quite different with the chiral expansion of B_π. Unlike F_π, B_π has very little mass dependence. Thus, the role of the NLO and NNLO analytic terms in the expansion of B_π is to cancel as much as possible the mass dependence brought by the non-analytic terms. When this is done correctly in an NLO fit, adding an NNLO term destabilizes the balance between analytic and non-analytic terms, therefore requiring a retuning of the LECs.

Putting together all of the information discussed up until now, we draw the following conclusions as to the range of applicability of $SU(2)$ χPT for $N_f = 2+1$ QCD. Note that conclusions may differ when considering applications to $N_f = 2$ QCD, since the latter is missing the relatively light degrees of freedom associated with the strange quark. As indicated in Table 2, our results for F_π have statistical uncertainties typically in the range of 0.5% to 2.2%, with a median error over our simulations of 1.2% and a standard deviation of 0.5%. Those for B_π are in the range of 0.3% to 3.3%, with a median and a standard error 0.8% and

0.7%. Similarly, the statistical uncertainties on m_{ud} and M_π^2 are in the ranges of 0.2% and 1.9% and of 0.4% and 3.2%, with medians and standard errors of $(0.4\%, 0.4\%)$ and (0.9%, 0.7%), respectively. For such results, we find that NLO χPT begins showing signs of failure for M_π beyond 300 MeV and breaks down completely around 450 MeV for both expansions. Adding NNLO terms allows one to describe consistently the mass dependence of F_π in the ξ-expansion, up to around 500 MeV, at the expense of NNLO corrections which are approaching those of the NLO ones. This is only marginally true in the x-expansion, as F and $\bar{\ell}_4$ begin deviating from the values given by the NLO fits with $M_\pi^{\max} \leq 300\,\text{MeV}$ in that expansion. However in both expansions, the addition of NNLO terms in B_π does not allow a description of that quantity beyond 300-350 MeV that is consistent with the NLO description at the level of around one standard deviation.

	x-expansion	ξ-expansion
	LO	
$B^{\rm RGI}$ [GeV]	$1.93 \pm 0.06 \pm 0.02$	$1.93 \pm 0.05 \pm 0.02$
F [MeV]	$88.1 \pm 1.3 \pm 0.3$	$87.9 \pm 1.4 \pm 0.3$
$[\Sigma^{\rm RGI}]^{1/3}$ [MeV]	$246.7 \pm 3.5 \pm 0.9$	$246.2 \pm 3.6 \pm 1.0$
	NLO	
$\bar{\ell}_3$	$2.38 \pm 0.4 \pm 0.3$	$2.7 \pm 0.6 \pm 0.4$
$\bar{\ell}_4$	$3.65 \pm 0.32 \pm 0.06$	$4.03 \pm 0.43 \pm 0.07$
	Other quantities	
F_π [MeV]	$92.9 \pm 0.9 \pm 0.2$	$92.9 \pm 0.9 \pm 0.2$
F_π/F	$1.054 \pm 0.006 \pm 0.002$	$1.058 \pm 0.007 \pm 0.002$

Table 3: *Results for LO and NLO LECs obtained from NLO, $SU(2)$ χPT fits in the x and ξ-expansion. We also give results for F_π and its ratio to F. The relevant χPT expressions are fitted to our lattice results for B_π and F_π with pion masses in the range* [120, 300] MeV. *In these results, the first error is statistical and the second is the systematic error in each expansion, computed as described in the text.*

4 Results for LECs and other physical quantities

Having explored the range in which one can describe the mass-dependence of the quantities B_π and F_π in $SU(2)$ χPT, we are now in a position to determine the corresponding LECs. We observe a small but significant change of behavior if we include points with pion masses above 300 MeV, which suggests that the NLO χPT expansion is beginning to break down beyond that point. Moreover, the inclusion NNLO terms does not seem to allow one to extend the range of applicability of χPT beyond that point, in particular for B_π. Thus, we will consider only NLO fits to determine the LO and NLO LECs, as well as quantities such as F_π or the condensate. Moreover, we will not include results with $M_\pi^{\rm max} > 300\,$MeV.

We begin by considering separately the results for the LECs and other physical quantities of interest in the x and ξ-expansion. They are given in Table 3. As described in Sec. 2, we consider all sources of systematic error. In particular, we consider 2 initial fit times in the two-point functions to account for possible excited state contributions ((8,9,11,13) / (9,11,13,15)), 2 mass cuts for the scale setting (380 / 480 MeV), 3 ways of performing the RI/MOM renormalization for Z_A and 6 for Z_S and different mass cuts in chiral fits (250 / 300 MeV). This implies a total of $2 \times 2 \times 3 \times 6 \times 2 = 144$ procedures for determining each quantity. We then weigh the result of each procedure by its p-value. This yields a distribution of results for each quantity. The distributions for the LO and NLO LECs are shown in Fig. 12 and Fig. 13, respectively. The central value for each quantity is chosen to be the mean of the distributions. Its systematic uncertainty is obtained by computing the variance. Finally, the statistical error is determined by repeating the construction of distributions for 2000 bootstrap samples, and considering the variance of their means around the central value.

In our approach, it is possible to decompose the systematic uncertainty into its various components. This is done by constructing systematic error distributions as above, but instead of considering a single distribution per observable, one constructs a separate distribution for each analysis variation associated with a given source of systematic uncertainty. For instance, for each quantity we have two distributions to estimate the uncertainty associated with the

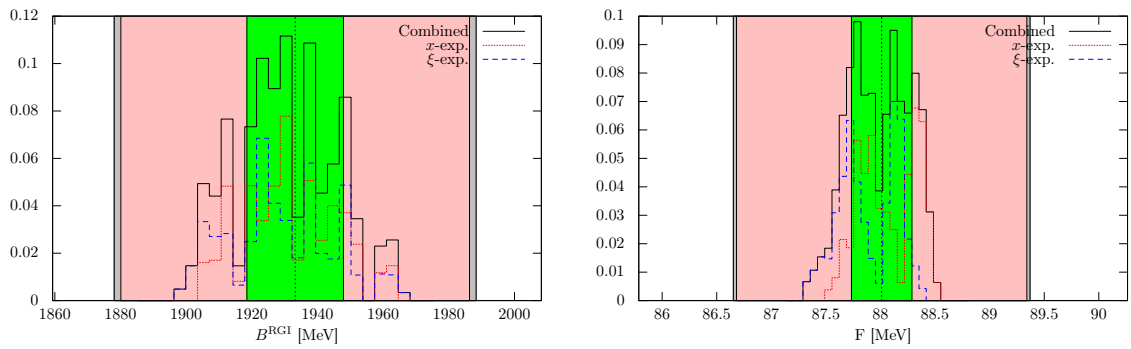

Figure 12: *Systematic error distributions for the LO LECs. These are obtained by varying the analysis procedure, as described in the text. The total distribution is delineated by the solid black line. It is the sum of the distributions corresponding to the analyses performed in the x and ξ-expansion. These are shown as a red dotted line and a blue dashed line, respectively. Where only the x or ξ-expansion distributions contribute, they partially hide the line corresponding to the total distribution. In the plots, the central, vertical, dotted line is the mean of the total distribution, i.e. our final central value. The central, vertical green band denotes the systematic error, the larger pink one, the statistical error and the largest gray one, the sum in quadrature of these two errors.*

choice of pion mass range, one for $M_\pi^{\rm max} = 250\,$MeV and another for 300 MeV. We then compute the mean of each of these distributions. The error associated with this source of systematic uncertainty is obtained from the variance of these means.

As Table 3 shows, the uncertainties on our results are dominated by statistical errors. This means that the numerical values of the contributions of each source of systematic uncertainty are not particularly relevant here. Nevertheless, for completeness, we provide a rough hierarchy of these contributions here. The dominant source for F, Σ and F_π is the pion-mass cut, followed by Z_S. The pion-mass cut also dominates the systematic error in $\bar{\ell}_3$, but is followed by the one associated with the choice of expansion (x versus ξ). The latter dominates in $\bar{\ell}_4$.

Let us now turn to a discussion of the results themselves. In both expansions, we determine the LO LECs with total uncertainties in the range of 1.5 to 2.9%. The pion decay constant is obtained even more precisely, with a total uncertainty of less than 1% and the uncertainty on F_π/F is as small as 0.7%. Of course the NLO LECs are obtained with significantly less precision: $\bar{\ell}_4$ has a total uncertainty of approximately 10% while for $\bar{\ell}_3$ it is around 25%.

The agreement of the results obtained from the x and ξ-expansions is striking. This is an additional confirmation that NLO $SU(2)$ χPT correctly describes M_π^2 and F_π up to $M_\pi \simeq 300\,$MeV. Indeed, the two expansions differ by higher order terms. This difference also explains why the agreement is better for LO LECs and F_π than it is for NLO LECs: the smaller, less constrained NLO contributions are more affected by changes made at higher orders.

Because of the consistency of the results in the two expansions, we combine them in the first column of Table 4 to obtain our final results. This combination is performed in a way which is entirely consistent with our determination of systematic errors. The two expansions (x / ξ) are treated as an additional alternative in our determination of LECs and other quantities. Thus, our final results are obtained from a total of $144 \times 2 = 288$ different

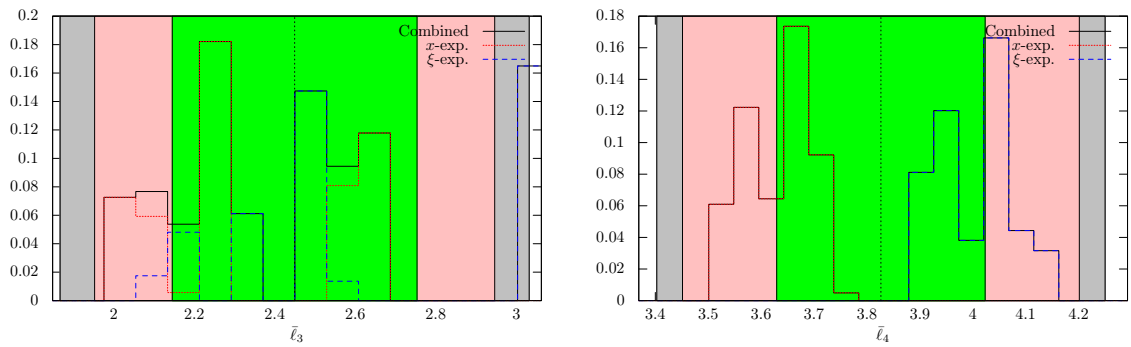

Figure 13: *Systematic error distributions for the NLO LECs. The different components of the graphs have the same meaning as in Fig. 12.*

analyses for each quantity. The corresponding systematic error distributions for the LECs are shown in Figs. 12–13, together with our final results for these quantities. It should be noted, however, that in performing fine comparisons between lattice studies, one may wish to compare them separately in each expansion.

The LO LECs and F_π do not change visibly compared to those obtained from the individual expansions. The systematic uncertainties on the NLO LECs increase slightly as a result of the variation induced by the use of the two expansions. For comparison, we give in the second column of Table 4 the averages for these quantities obtained by FLAG [11] and/or the PDG [46].

We now turn to a comparison of our results with those of other collaborations who have performed $N_f \geq 2+1$ studies [2, 6, 7, 13–20]. Note that amongst those, the only study which includes simulations all the way down to the physical value of the pion mass is the staggered fermion one in [6]. That study computes the LO quantities $2Bm_{ud}^{\rm ph}$ and F_π/F, and the NLO LECs $\bar{\ell}_3$ and $\bar{\ell}_4$. Thus, in addition to the physical value of M_π, it requires F_π to determine the LO LEC F and the renormalized quark mass, $m_{ud}^{\rm ph}$, to determine the other LO LEC, B, or alternatively the quark condensate. It takes the former from [46] and the latter from [4, 5], which make use of the same Wilson quark simulations as employed in the present paper, and is thus not fully de-correlated from the results presented here. Moreover, the use of outside input for F_π and $m_{ud}^{\rm ph}$ forbids predicting these two quantities and thus making valuable crosschecks of the calculation. It may also be noted that the smallest lattice spacing in that work is 0.1 fm.

We find agreement with [6] on the LO LECs F and B. MILC [17] obtains a condensate which is more than one standard deviations larger than ours while RBC/UKQCD [7] find a value which is more than two standard deviations smaller than ours. As for F, it is not studied by RBC/UKQCD, but agreement with MILC [17] is excellent, while ETM [19], in an $N_f = 2+1+1$ computation, find a value which is more than 1.5 combined standard deviations smaller than ours. Regarding F_π/F, which measures the chiral corrections to F_π at $M_\pi^{\rm ph}$, our result is in good agreement with that of Borsanyi *et al.* [6], NPLQCD [18] and MILC [17]. However, ETM's $N_f = 2+1+1$ result [19] is almost 2.5 standard deviations way from ours.

It is interesting to note that the deviations from ETM's [19] results gradually decrease as we increase $M_\pi^{\rm max}$ above 300 MeV. This is clearly visible in the right panel of Fig. 6 which shows that F decreases by more than one standard deviation when lattice results with $M_\pi \gtrsim 350\,$MeV are included. Though we have not shown the $M_\pi^{\rm max}$ dependence of F_π/F, it

	Combined	FLAG & PDG
	LO	
$B^{\rm RGI}$ [GeV]	$1.93 \pm 0.06 \pm 0.02$	
$B^{\overline{\rm MS}}(2\,{\rm GeV})$ [GeV]	$2.58 \pm 0.07 \pm 0.02$	
F [MeV]	$88.0 \pm 1.3 \pm 0.3$	86.4 ± 0.7 [11, 46]
$[\Sigma^{\rm RGI}]^{1/3}$ [MeV]	$246.5 \pm 3.5 \pm 0.9$	244 ± 16
$[\Sigma^{\overline{\rm MS}}(2\,{\rm GeV})]^{1/3}$ [MeV]	$271 \pm 4 \pm 1$	269 ± 18 [11]
	NLO	
$\bar{\ell}_3$	$2.5 \pm 0.5 \pm 0.4$	3.2 ± 0.8 [11]
$\bar{\ell}_4$	$3.8 \pm 0.4 \pm 0.2$	4.4 ± 0.2 [12]
	Other quantities	
F_π [MeV]	$92.9 \pm 0.9 \pm 0.2$	$92.21 \pm 0.02 \pm 0.14$ [46]
F_π/F	$1.055 \pm 0.007 \pm 0.002$	1.073 ± 0.015 [12]

Table 4: *Our final results for LO and NLO LECs, as well as for F_π and its ratio to F. They are obtained by combining the results leading to those given for the individual x and ξ-expansion, as described in the text. In these results, the first error is statistical and the second is systematic. The computation of these errors is described in the text. The conversion of RGI numbers to those in the $\overline{\rm MS}$ scheme at 2 GeV is performed using the results of [5]. For comparison, we give in the second column the estimates of the FLAG review [11] for the LECs and F_π/F, and of the PDG [46] for F_π. Note that an update of the FLAG review is planned, of which a preliminary version can be found at [47].*

undergoes a very similar increase, instead of decrease. This suggests that the discrepancy that we observe with ETM [19] on F and F_π/F may be due to the fact that ETM's lightest pion is 270 MeV and that they include points up to 510 MeV in their NLO fits. This observation is further corroborated by the discussion in Sec. 5.2, where we investigate the effect of removing lattice data at the low-M_π end.

For completeness we note that B undergoes a more than one standard deviation increase when lattice results with $M_\pi \gtrsim 350\,{\rm MeV}$ are included. The net effect is that Σ remains essentially stable as $M_\pi^{\rm max}$ is increased.

We now discuss NLO LECs. Our results for $\bar{\ell}_3$ and $\bar{\ell}_4$ are systematically smaller than those obtained in other recent $N_f \geq 2+1$ computations [2, 6, 7, 13–20], the effect being more pronounced in the x-expansion which is the one used in other studies. Though the discrepancy is generally marginal, it is marked with the $N_f = 2+1+1$ ETM results [19]. Their results for $\bar{\ell}_3$ and $\bar{\ell}_4$ are almost two combined standard deviations above ours. As Fig. 7 shows, these larger values are compatible with those which we obtain including points with $M_\pi \gtrsim 350\,{\rm MeV}$. Thus, the possible explanation for the discrepancy with ETM's LO LECs also applies for NLO LECs. The only other results obtained with simulations down to the physical pion mass [6] are also larger than ours, though the difference here is within a standard deviation.

We conclude this section with a discussion of NNLO LECs. The results presented here should be taken with a grain of salt. The first reason is that we are only sensitive to them if we include points with $M_\pi \geq 400\,{\rm MeV}$. While NNLO χPT for F_π may be applicable for such masses, this is not the case for B_π. Moreover, the statistical uncertainties on these results are very large. Nevertheless, because very little is known about these LECs, we believe that the information brought by our analysis is useful. We obtain these estimates very much in

the same way as we determine the LO and NLO LECs. The only difference is that instead of considering $M_\pi^{\max} = 250$ and 300 MeV, we estimate systematic errors associated with the neglect of higher-order terms using $M_\pi^{\max} = 400$, 450 and 500 MeV. Note that for these ranges, the p-values of the NNLO fits are good, as shown in Fig. 5.

The results that we obtain are, for the x-expansion, $k_M = -2.4 \pm 5.3 \pm 2.8$ and $k_F = 4.4 \pm 4.3 \pm 2.1$, and $c_M = 37. \pm 12. \pm 13.$ and $c_F = 20. \pm 15. \pm 17.$ for the ξ-expansion. The only other lattice study in which k_M and k_F are considered is [6]. As already noted this study uses the physical value of F_π as input. Moreover, the NNLO fits are constrained with a prior on $\bar{\ell}_{12}$, and in some cases on k_M and k_F. Considering only the fits in which k_M and k_F are not constrained, they find $k_M \sim 2$ and $k_F \sim 1$.

As already mentioned, our NNLO fits are sensitive to the combination of NLO LECs, $\bar{\ell}_{12} = (7\bar{\ell}_1 + 8\bar{\ell}_2)/15$. We determine it in the same way as the NNLO LECs, finding $\bar{\ell}_{12} = 3.0 \pm 1.1 \pm 0.9$ and $5.5 \pm 1.3 \pm 0.9$ in the x and ξ-expansion, respectively. The ξ-expansion leads to a larger value of that LEC, the discrepancy probably indicating a sensitivity to the treatment of higher-order terms. Since we have no reason to favor the result of one expansion over that from the other, we include the results from both in our final estimate of $\bar{\ell}_{12}$. In this way, we find $\bar{\ell}_{12} = 3.9 \pm 1.1 \pm 1.5$. For comparison we can use the LECs $\bar{\ell}_1$ and $\bar{\ell}_2$ obtained from the fitting of NLO expansions of $\pi\pi$ scattering amplitudes to experimental data [12]. Combining the results for $\bar{\ell}_1$ and $\bar{\ell}_2$ from [12], one obtains $\bar{\ell}_{12} = 2.1 \pm 0.3$. It should be noted that the results in [12] only include uncertainties coming from the phenomenological input and not possibly-significant uncertainties coming from neglected higher-order terms in the relevant chiral expansion. Though our determination from NNLO fits have much larger errors, it is compatible with the value from $\pi\pi$ scattering.

We have also performed NNLO fits imposing a Gaussian constraint on $\bar{\ell}_{12}$. Instead of taking $\bar{\ell}_{12} = 2.1 \pm 0.3$ as done in [6], we more than triple the error and consider $\bar{\ell}_{12} = 2.1 \pm 1.0$. The fits still have good p-values. However, even such a loose prior has a significant impact on the LECs present at NNLO. Instead of the values given above, with this prior we find $k_M = -0.1 \pm 1.3 \pm 0.9$, $k_F = 3.0 \pm 1.8 \pm 0.4$ and $\bar{\ell}_{12} = 2.15 \pm 0.05 \pm 0.11$ for the x-expansion, and $c_M = 3. \pm 4. \pm 3.$, $c_F = 14. \pm 9. \pm 4.$ $\bar{\ell}_{12} = 2.15 \pm 0.03 \pm 0.03$ for the ξ-expansion. Perhaps more surprisingly, this prior also affects the NLO LECs extracted from NNLO fits. Determining these LECs from the three pion-mass intervals with $M_\pi^{\max} = 400$, 450 and 500 MeV leads to $(\bar{\ell}_3, \bar{\ell}_4) = (2.8 \pm 0.4 \pm 0.3, 3.83 \pm 0.28 \pm 0.05)$ for the x-expansion and $(\bar{\ell}_3, \bar{\ell}_4) = (2.5 \pm 0.6 \pm 0.4, 3.3 \pm 0.5 \pm 0.2)$ in the ξ-expansion with the prior. This is to be compared with $(\bar{\ell}_3, \bar{\ell}_4) = (3.9 \pm 1.3 \pm 1.2, 4.2 \pm 0.5 \pm 0.4)$ for the x-expansion and $(\bar{\ell}_3, \bar{\ell}_4) = (5.1 \pm 1.2 \pm 0.8, 4.1 \pm 0.5 \pm 0.3)$ in the ξ-expansion obtained without prior. Not surprisingly, the difference observed in the ξ-expansion also carries over to F_π/F which is significantly lower with the constraint. More generally, while the x-expansion results with and without prior are consistent within errors, those in the ξ-expansion are not. This is due to the fact that, without a Gaussian constraint, our NNLO, ξ-expansion fits favor a larger value of $\bar{\ell}_{12}$. Needless to say that a more stringent constraint on $\bar{\ell}_{12}$ or forcing the NNLO LECs to vanish within a few units will have an even larger impact. Thus, while we cannot exclude the use of priors based solely on the absolute quality of the fits which include them, we take the differences that we observe when they are added as a warning. The use of even loose priors may induce one to believe that data has more resolution power than it actually has and may bias the results obtained.

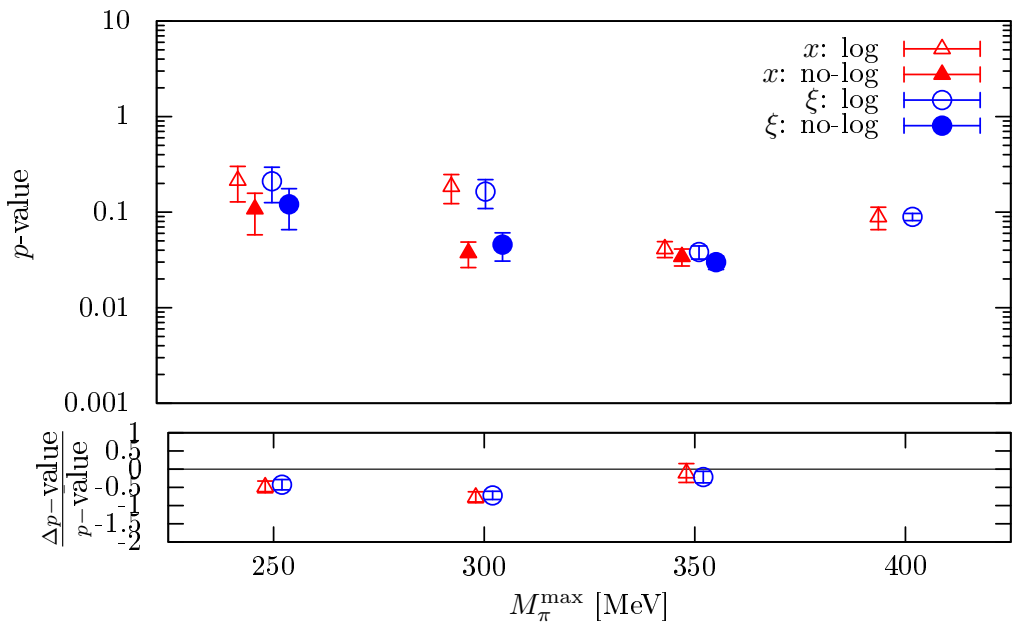

Figure 14: *Comparison of the p-values obtained in fits of NLO $SU(2)$ expansion, including and omitting the chiral logarithms. These fully correlated fits to our lattice results for B_π and F_π include points whose pion mass is in the range $[120\,\text{MeV}, M_\pi^{\max}]$. Results are shown for the x and ξ-expansion. In the top panel the individual p-values are shown. Those of fits including the logarithms are the same as the ones given in Fig. 5. In the lower panel it is the difference of the p-value obtained omitting logarithms minus the χPT one, normalized by the latter. Error bars on each point are the systematic uncertainties discussed in Sec. 3.2. For the sake of clarity, results are shifted about the values of $M_\pi^{\max} = 250, \cdots$ MeV, at which they are obtained.*

5 On the presence of chiral logarithms and the possible misuse of χPT

5.1 On the presence of NLO chiral logarithms

Having studied the range of applicability of the NLO expansions, we now explore the extent to which chiral logarithms are required to describe our results. We do so by fitting, to our results for B_π and F_π, the NLO expressions in Eq. (14) and Eq. (15), with the logarithms omitted. As in our study of the range of applicability of $SU(2)$ χPT, we include in these fully correlated fits all points with $m_{ud} \leq m_{ud}^{\max}$ or $M_\pi \leq M_\pi^{\max}$, and study the behavior of the p-value as the cut is increased. We also monitor the value of F_π at M_π^{ph}.

In Fig. 14 we compare these p-values of NLO fits without logarithms to those of the NLO χPT fits performed in Sec. 3, both in the x and ξ-expansion. The p-values obtained when logarithms are omitted are consistently lower than for the χPT fits, though they remain acceptable for $M_\pi^{\max} \leq 350\,\text{MeV}$. Beyond that point they become very bad. To determine the significance of the preference for the presence of logarithms, we compute the difference of the p-values obtained omitting the chiral logarithms to those including them, normalized by the latter. These are shown in the lower panel of Fig. 14. As the figure shows, in the range

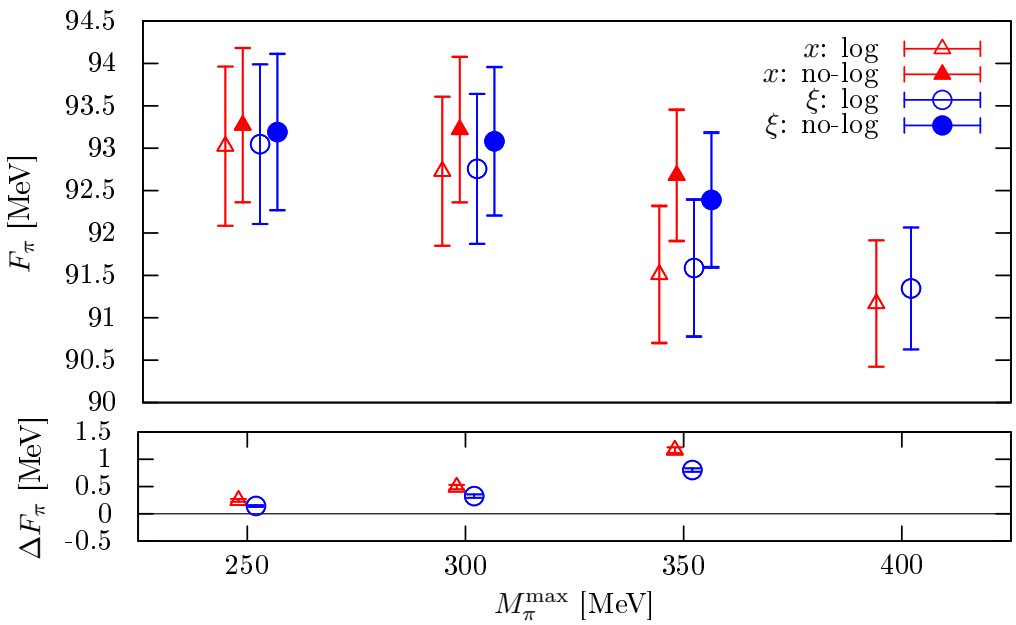

Figure 15: *F_π as a function of $M_\pi^{\max}$, obtained from NLO fits with and without and logarithms, in the x and ξ-expansion (upper panel). In the lower panel it is the difference (no log. minus log.) of these highly correlated results that are shown. Error bars on each point are the statistical and the quadratically combined statistical-plus-systematic uncertainties. For the sake of clarity, results are shifted about the values of $M_\pi^{\max} = 250, \cdots$ MeV, at which they are obtained.*

of applicability of NLO χPT, i.e. $M_\pi^{\max} \leq 300\,\text{MeV}$, the presence of logarithms is favored by about five to eight standard deviations in the p-value in both expansions.

Fig. 15 shows the $M_\pi^{\max}$ dependence of the value of F_π at physical M_π, obtained in fits with and without logarithms. Both fits give very similar results in the range of applicability of NLO χPT, where $M_\pi^{\max} \leq 300\,\text{MeV}$. Thus, at our level of accuracy, a simple linear interpolation would allow us to obtain F_π. However, the bottom panel of Fig. 15 shows that this will no longer be true when the total uncertainty on F_π reaches a few tenths of an MeV.

To conclude this discussion, our lattice results clearly favor the presence of logarithms in the range of applicability of NLO $SU(2)$ χPT, though the values of F_π obtained without them are compatible with those obtained in χPT at the present level of accuracy.

5.2 On the possible misuse of χPT

In this section we examine the role of lattice results near the physical value of M_π, for the determination of LECs. For this purpose we fix the maximum value of M_π to $M_\pi^{\max} = 450\,\text{MeV}$ and study the dependence of the p-value and of the LECs as a function of the lower bound, $M_\pi^{\min}$, that we place on the lattice results included in the fit. We consider fully correlated NLO, $SU(2)$ χPT fits, both in the x and ξ-expansion. We compare the results obtained to those given by NLO fits in our canonical range, $M_\pi \in [120, 300]\,\text{MeV}$. We perform the comparison by subtracting these canonical results for the LECs from the new ones, under our systematic and bootstrap error loops. Thus we obtain fully controlled statistical and

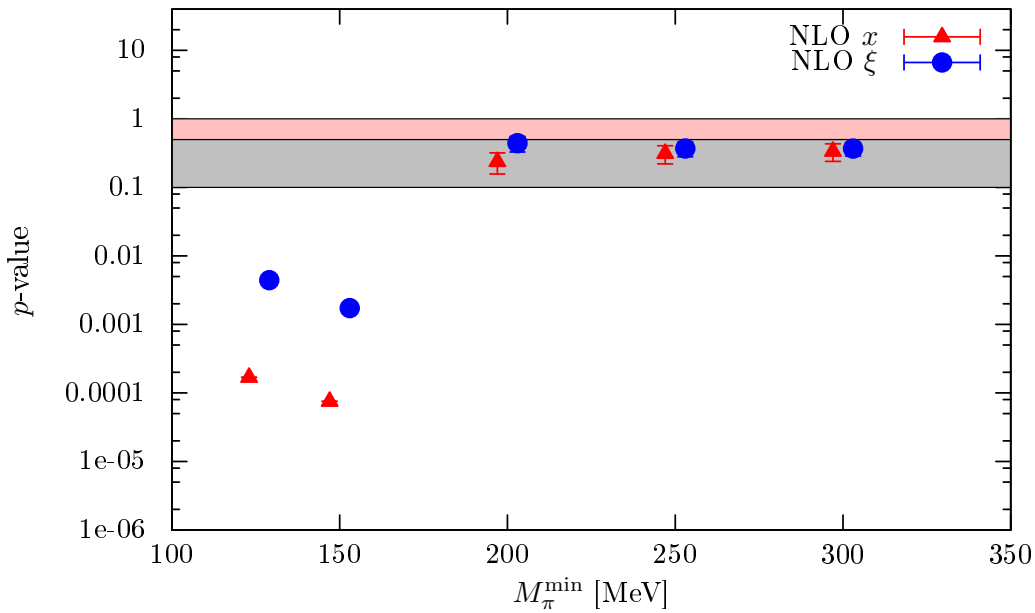

Figure 16: *p-value as a function of $M_\pi^{\min}$. The p-values are obtained by performing fully correlated NLO, $SU(2)$ χPT fits to lattice results for B_π and F_π with pion masses in the range $[M_\pi^{\min}, 450\,\text{MeV}]$. Both the x and ξ-expansion are considered. The points with $M_\pi^{\min} = 120, \cdots$ MeV are the same as those with $M_\pi^{\max} = 450, \cdots$ MeV in Fig. 5. The horizontal bands have the same meaning as in Fig. 5. Error bars on each point are the systematic uncertainties discussed in Sec. 3.2. For the sake of clarity, results are shifted about the values of $M_\pi^{\min} = 120, \cdots$ MeV, at which they are obtained.*

systematic errors on these differences.

In Fig. 16 we plot the p-value of these NLO fits as a function of $M_\pi^{\min}$ with full systematic errors. We find acceptable values for $M_\pi^{\min} \geq 200\,\text{MeV}$, which may give the erroneous impression that NLO, $SU(2)$ χPT is applicable in the range $M_\pi \in [200, 450]\,\text{MeV}$. However, as we showed in Sec. 3.2, NLO χPT is not applicable up to 450 MeV.

To give an idea of how one might be misled in the determination of LECs and physical quantities, in Fig. 17 we plot the LO LECs and F_π as a function of $M_\pi^{\min}$ for $M_\pi^{\min} \in [150, 300]\,\text{MeV}$, for both the x and ξ-expansion. As in Figs. 6–7, we also plot, in the lower panel, the difference of these quantities with the corresponding results obtained in our canonical range $M_\pi \in [120, 300]\,\text{MeV}$. While B remains close to its physical value, F and F_π drop significantly below their correct values, by as much as 7%. The net result on the condensate, Σ, is even larger since $\Sigma = F^2 B$.

Fig. 18 displays the same study, but for NLO LECs. While the value of $\bar{\ell}_3$ remains compatible with its physical value, $\bar{\ell}_4$ increases steadily as $M_\pi^{\min}$ is increased, especially in the ξ-expansion. These are the NLO expression of the observations made at LO. In particular, the larger values of $\bar{\ell}_4$, or equivalently of the scale Λ_4, indicate that as lattice results at lower M_π are removed, the downward trend of the chiral logarithm in F_π, as the chiral limit is approached, is allowed to begin at larger values of M_π. The end result is lower values of F and F_π for larger $M_\pi^{\min}$. These results fully corroborate the observations that we made, in

Sec. 4, about the values of LECs obtained by groups whose simulations do not reach down to small $M_\pi < 200\,\mathrm{MeV}$.

To summarize, if NLO $SU(2)$ χPT is applied to results for B_π and F_π up to $M_\pi^{\max} = 450\,\mathrm{MeV}$, one obtains a good description if one does not have results very close to the physical point, i.e. with $M_\pi < 200\,\mathrm{MeV}$. Thus, one may be led to believe that one is in the range of applicability of NLO χPT. However, as we show, the description of F_π, in particular, is significantly different from that obtained around the physical point, with values of F and F_π which are too small and of $\bar{\ell}_4$ which are too large. Said differently, results for F_π close to the physical point show less downward curvature than results at larger values of M_π suggest.

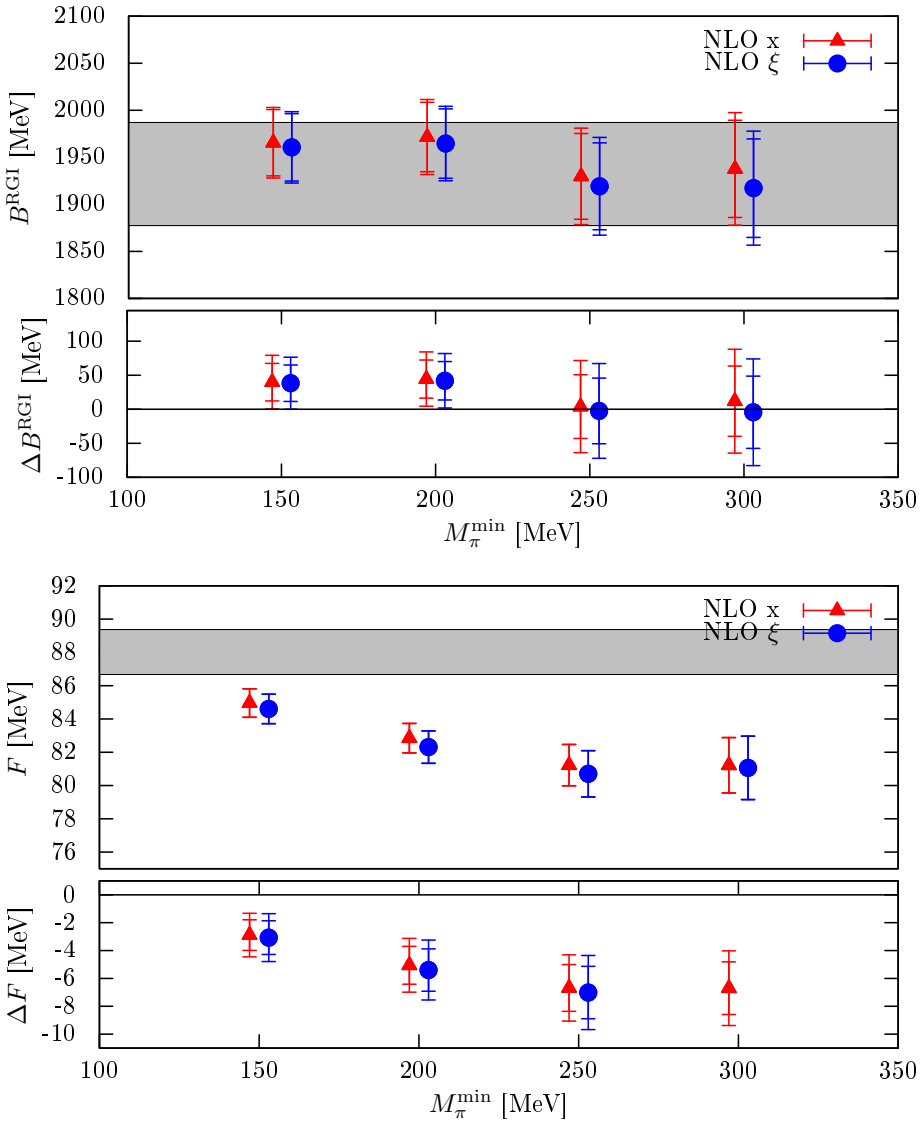

Figure 17: *LO LECs as a function of $M_\pi^{\rm min}$ (upper panel of each plot). The LECs are obtained from the fits described in Fig. 16. The horizontal gray band denotes our final result for the corresponding LEC, given in Table 4, and obtained as described in Sec. 4. In the lower panel corresponding to each LEC, it is the difference of this LEC with the one obtained from fits in our canonical range, $M_\pi \in [120, 300]$ MeV. Error bars on each point are the statistical and the quadratically combined statistical-plus-systematic uncertainties. For the sake of clarity, results are shifted about the values of $M_\pi^{\rm min} = 150, \cdots$ MeV, at which they are obtained.*

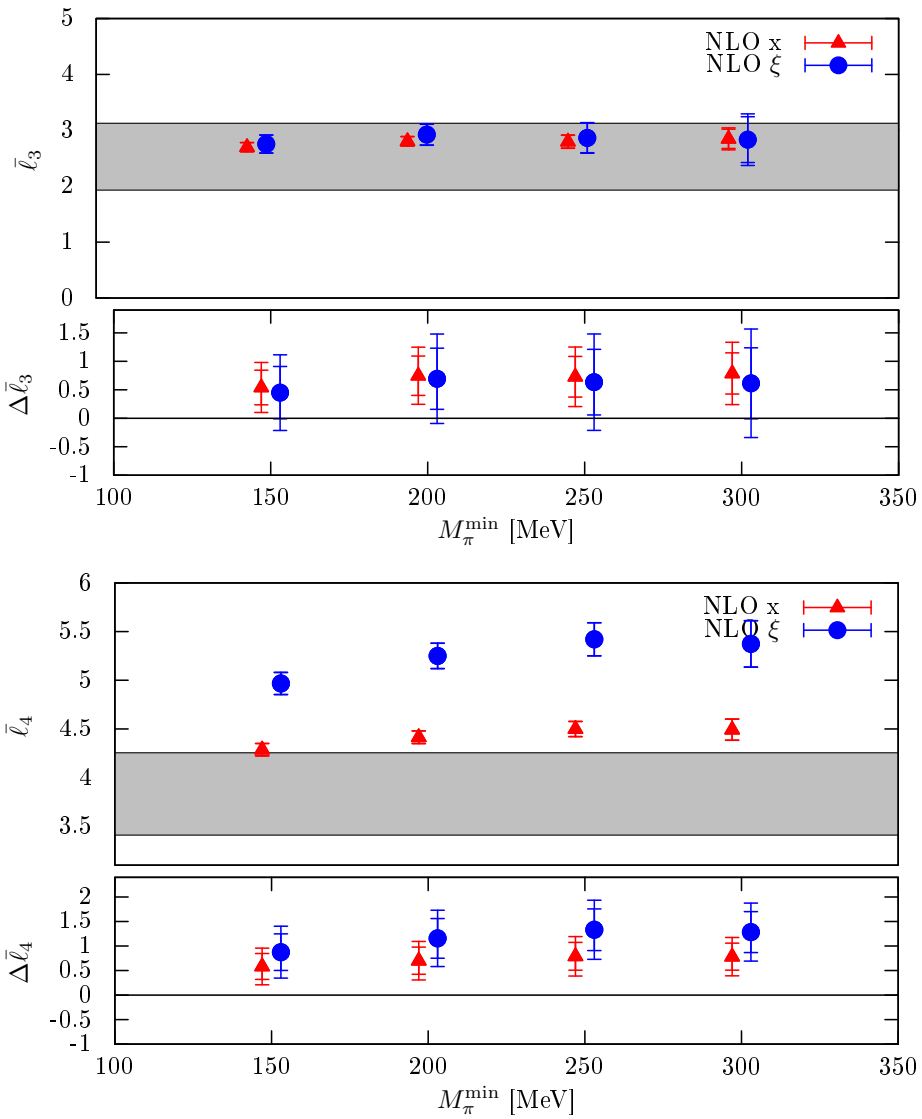

Figure 18: *Same as Fig. 16, but for NLO LECs.*

6 Conclusion

We have performed a detailed, fully-correlated study of the chiral behavior of the pion mass and decay constant, based on 2+1 flavor lattice QCD simulations. These calculations are implemented using tree-level, $O(a)$-improved Wilson fermions all the way down to $M_\pi \simeq 120\,\text{MeV}$. This coverage of the low-mass region allows to probe deeply into the chiral regime. Quark masses and decay constants undergo fully-controlled nonperturbative renormalization. Moreover, our fine lattice spacings down to 0.054 fm and large volumes up to 6 fm enable us to accurately perform the relevant continuum and infinite-volume extrapolations. We set the scale of our calculations with the Ω baryon mass, which is independent of the quantities of interest here. This allows us to make valuable tests of our calculation. The first is an *ab initio* computation of F_π, whose result agrees well with experiment [46] within our 1% error bar. The second is a determination of m_{ud} that is fully compatible with the FLAG value [11]. In fact, it is nearly identical to the result of [4, 5], which is not surprising as our treatment of quark masses is carried over from that work.

We begin the study presented in this paper with a systematic investigation of the range of applicability of $SU(2)$ χPT. We consider two expansions. The first, which is that used in previous $N_f \geq 2+1$ studies [2, 6, 7, 13–20], is in quark mass (x-expansion). The second is in squared pion mass (ξ-expansion) and has not, as far as we know, been investigated before. The study of the later has led us to find constraints on the NLO LEC $\bar{\ell}_4$ in terms of the LO LEC F and bounds on the NNLO LEC c_F in terms of the F and the NLO LECs $\bar{\ell}_4$ and $\bar{\ell}_{12}$ defined in and around Eq. (5). These bounds are derived and discussed in Appendix A.

To explore the range of applicability of $SU(2)$ χPT we consider a number of criteria. These include a study of the p-value of our combined, fully-correlated χPT fits, to M_π^2 and F_π, as a function of $M_\pi^{\max}$, where $[120\,\text{MeV}, M_\pi^{\max}]$ is the range of the masses of the lattice pions which we include in our fits. We also study the values of the LO, NLO and NNLO LECs obtained in these fits, as a function of $M_\pi^{\max}$. We further investigate the relative size of contributions of different orders in the χPT expansion for different pion masses. While our study of NLO expansions is well controlled, we find that we do not really have enough precision to make definite statements about NNLO.

Our systematic investigation leads to the following conclusions. We find that NLO χPT for M_π^2 and F_π begins showing signs of failure for M_π beyond 300 MeV and breaks down completely around 450 MeV for both expansions. Adding NNLO terms allows one to describe consistently the mass dependence of F_π in the ξ-expansion, up to around 500 MeV, at the expense of NNLO corrections which are approaching those of the NLO ones. This is only marginally true in the x-expansion, as F and $\bar{\ell}_4$ begin deviating from the values given by the NLO fits with $M_\pi^{\max} \leq 300\,\text{MeV}$ in that expansion. However in both expansions, the addition of NNLO terms in B_π does not allow a description of that quantity beyond 300-350 MeV that is consistent with the NLO description at the level of around one standard deviation. This behavior is consistent with the fact that these are asymptotic expansions. Since conclusions about applicability of $SU(2)$ χPT depends not only on the range of pion masses, but also on the precision of the results to which it is applied, it is important that the latter be specified. This is discussed in detail in Sec. 3.4. Here we only remind the reader that the typical precision of our lattice results is around 1%. Note also that conclusions may differ when considering applications of $SU(2)$ χPT to $N_f = 2$ QCD, since the latter is missing the relatively light degrees of freedom associated with the strange quark.

Having established the range of applicability of $SU(2)$ χPT, which is very similar for both

expansions, we use lattice results in that range to determine the theories' LECs. In particular, we use our combined, fully-correlated NLO χPT fits to lattice results for M_π^2 and F_π with $M_\pi^{\max} \leq 300\,\text{MeV}$, to compute F, B, $\bar{\ell}_3$ and $\bar{\ell}_4$, as well as the quark condensate and F_π, with fully controlled uncertainties. Our final results are summarized in Table 4 and those for the individual x and ξ-expansions in Table 3. A detailed comparison with the $N_f \geq 2+1$ studies of [2, 6, 7, 13–20] is given in Sec. 4. Here we note that while our results for $\bar{\ell}_3$ and $\bar{\ell}_4$ are consistent with those obtained from lattice $N_f \geq 2+1$ simulations with pion masses below 200 MeV [6, 7, 17], they are systematically smaller, particularly those obtained in the x-expansion, which is used by all other collaborations. It is also interesting to note that our result for the quark condensate has an uncertainty which is almost 5 times smaller than the latest FLAG compilation of [11].

We investigate the application of NNLO $SU(2)$ χPT to our lattice results. There we find that we have to include results with M_π at least up to 400 MeV to have enough information to stabilize these fits without imposing arbitrary priors. Unfortunately, our studies suggest that, at such masses, we are already reaching beyond the range of applicability of NNLO $SU(2)$ χPT. Nevertheless, since little is known about NNLO LECs, we still attempt to determine them, with results given at the end of Sec. 4. As noted there, these results should be taken with a grain of salt and are only meant as indicative.

In Sec. 5 we explore the presence of NLO chiral logarithms in our lattice results. We show that this presence is significantly favored in the region of applicability of NLO $SU(2)$ χPT. While the inclusion of logarithms does not make a significant difference on the value of F_π obtained at the present level of accuracy, we find that it will when the total uncertainty on F_π reaches a few tenths of an MeV.

In this same section, we examine the role of lattice results near the physical value of M_π, in particular for the determination of LECs. We find that one obtains perfectly good NLO fits of lattice results for M_π^2 and F_π in the range $[M_\pi^{\min}, 450\,\text{MeV}]$ with $M_\pi^{\min} \geq 200\,\text{MeV}$. This might lead one to believe that NLO $SU(2)$ χPT is applicable in this range. However, our systematic study of the range of applicability of this theory already showed that the theory failed for $M_\pi \gtrsim 450\,\text{MeV}$. Moreover, while the value of B and $\bar{\ell}_3$ are not strongly affected by considering higher pion mass ranges, this is not true of F, $\bar{\ell}_4$, the pion decay constant and the quark condensate.

Acknowledgments

We thank Alberto Ramos for his help in the early stages of this project. Jérôme Charles and Marc Knecht are thanked for helpful conversations. Computations were performed using HPC resources provided by GENCI-[IDRIS] (grant 52275) and FZ Jülich, as well as using clusters at Wuppertal and CPT. This work was supported in part by the OCEVU Excellence Laboratory, by CNRS grants GDR $n^0$2921 and PICS $n^0$4707, by EU grants FP7/2007-2013/ERC $n^0$208740, MRTN-CT-2006-035482 (FLAVIAnet) and by DFG grants FO 502/2, SFB-TR 55.

Appendix A Solution for F_π in the ξ-expansion and ensuing constraints

As mentioned in Sec. 3.1, the expressions for F_π in the ξ-expansion are obtained by solving the second equation in (7) for F_π. At NLO this equation is quadratic and, at NNLO, it is quartic. Therefore, it has either up to 2 or 4 solutions and there is no guarantee that any of them are physical. In this section we investigate the conditions under which a physical solution exists. At fixed order in χPT, we find that these conditions impose non-trivial constraints on the LECs. Of course, if higher orders are allowed, these constraints eventually disappear.

The second equation in (7) can be rewritten as

$$f(r) \equiv r^4 - r^3 - Cr^2 - D = 0 \ , \tag{17}$$

with

$$C = X \ln\left(\frac{\Lambda_4}{M_\pi}\right)^2 , \qquad D = \frac{X^2}{4}\left\{\left[\ln\left(\frac{\Omega_F}{M_\pi}\right)^2\right]^2 - 4c_F\right\} \ , \tag{18}$$

and

$$r = \frac{F_\pi}{F}, \qquad X = \left(\frac{M_\pi}{4\pi F}\right)^2 \ . \tag{19}$$

At NLO, $D = 0$ and, since $F_\pi = 0$ is not physical, Eq. (17) reduces to the quadratic equation

$$r^2 - r - C = 0 \ . \tag{20}$$

This equation has real solutions iff $C \geq -1/4$ or

$$\bar{\ell}_4 \geq \ln\left(\frac{M_\pi}{\hat{M}_{\pi^+}}\right)^2 - \left(\frac{2\pi F}{M_\pi}\right)^2 \ . \tag{21}$$

Since we want $F_\pi \geq F/2$, the physical solution is the larger of the two, i.e.

$$F_\pi = \frac{F}{2}\left[1 + \sqrt{1+4C}\right] \ . \tag{22}$$

Note that F_π is greater than F iff $C > 0$ or, equivalently for $M_\pi \geq \hat{M}_{\pi^+}$, $\bar{\ell}_4$ is positive and its contribution in (7) dominates over that of the chiral logarithm. Thus, the constraint in Eq. (21) is weaker than requiring that $F_\pi > F$. On the other hand, the validity of NLO χPT would generically require that $|C| \ll 1$. From that perspective, the constraint of Eq. (21), $C \geq -1/4$ is a little more specific, since it tells us that a positive NLO correction in (7), whose magnitude is more than 25%, is not allowed if one assumes that the NLO ξ-expansion of F_π is exact. Assuming that this is the case, as we do when we fit our lattice results to this expression, Eq. (17) imposes a constraint on the NLO LEC, $\bar{\ell}_4$, in terms of the LO LEC, F, and of the pion mass at which the NLO ξ-expression is applied. Note that the RHS of Eq. (21) is a monotonically increasing function of M_π, indicating that the constraint on $\bar{\ell}_4$ becomes more and more stringent as one tries to apply NLO ξ-expressions to more and more massive pions. In particular, if we assume that the expansion must hold up to a value of $M_\pi = M_\pi^{\max}$, the lower bound on $\bar{\ell}_4$ that must be enforced is the value of the RHS at $M_\pi^{\max}$. We impose this lower bound dynamically in the NLO, ξ-expansion fits which are described in Sec. 3.1.

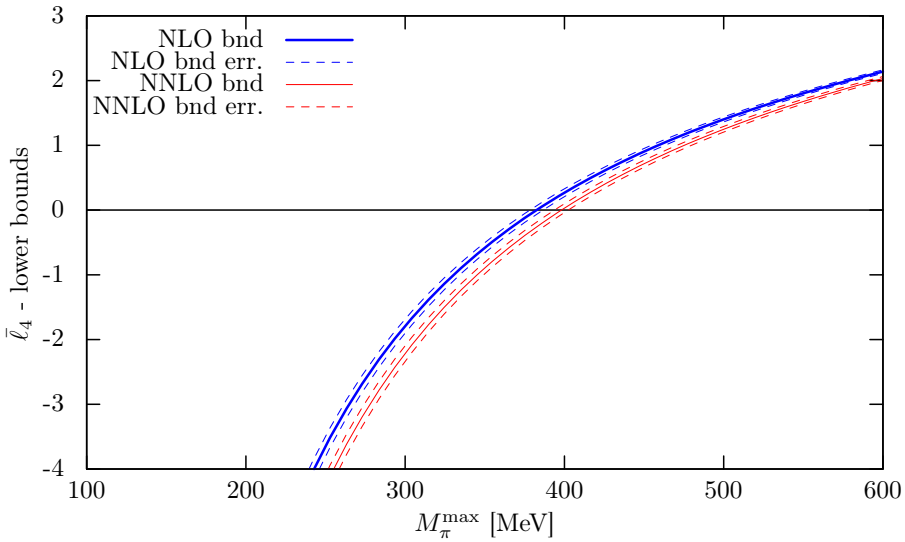

Figure 19: *Illustration of the NLO and NNLO lower bounds on $\bar{\ell}_4$ coming from the requirement that there is a physical solution for F_π assuming that the NLO or the NNLO ξ-expansion expressions of (7) hold exactly. $\bar{\ell}_4$ must lie above the given curve for each order in the expansion. To plot these curves, we use our final result for F given in Table 4. The dashed curves delimit the 1σ error band on each bound arising from the total uncertainty on F.*

For illustration, in Fig. 19 we plot this bound and its uncertainty as a function of $M_\pi^{\max}$. The curves correspond to our final result for F, given in Table 4. This bound is rather weak. It requires that $\bar{\ell}_4$ must be positive if one wants a physical solution above $M_\pi \sim 400\,\text{MeV}$ at NLO in the ξ-expansion and larger than 4 only for $M_\pi^{\max} \gtrsim 1.1\,\text{GeV}$. The latter indicates that the NLO fit of our data that we perform for $M_\pi^{\max} = 300\,\text{MeV}$ cannot be extended up to 1.1 GeV. While our study shows that there are many other important reasons for why this is the case, it is still interesting that fixed-order ξ-expansions have a built-in maximum pion-mass range.

At NNLO, Eq. (17) for F_π is quartic and therefore has up to 4 solutions. Moreover, it is easy to show that $f(r)$ has 3 extrema, one of which is at $r = 0$. There are two other real extrema iff

$$\bar{\ell}_4 \geq \ln\left(\frac{M_\pi}{\hat{M}_{\pi^+}}\right)^2 - \frac{9}{8}\left(\frac{2\pi F}{M_\pi}\right)^2 , \tag{23}$$

which is slightly less constraining than Eq. (21). Thus, for any pion-mass range, the NNLO ξ-expansion admits slightly smaller values of $\bar{\ell}_4$ than does the NLO expansion. This is not surprising as we know that bounds on the LECs must disappear in the limit of infinite order. However, finding such a value would imply that the NLO expansion is only applicable in a smaller mass range than the NNLO one. In turn, this would be a sign that χPT is having trouble.

Now let us consider the possibility that $r = 0$ is the only real extremum, i.e. that $C < -9/32$. Because of the signs of the terms in $f(r)$, it must be a minimum. Since we want a solution to Eq. (17) such that $F_\pi > F$, we must have $|D| > |C|$. But for this to be true, the NNLO term in the ξ-expansion must be larger than the NLO term. In that case the

ξ-expansion has clearly broken down, which is not an option of interest here. Thus we assume that (23) is satisfied, so that $f(r)$ has 3 real extrema. It is then straightforward to convince oneself that the absolute minimum of $f(r)$ is at $r_+ = (3+\sqrt{9+32C})/8$. Therefore, Eq. (17) will have at least one real solution for F_π iff $f(r_+) \leq 0$. This translates into a lower bound on the NNLO LEC c_F, in terms of the LO and NLO LECs, F, $\bar{\ell}_4$ and $\bar{\ell}_{12}$. This upper bound is not necessarily a monotonic function of M_π. Therefore, unlike the lower bound of Eq. (23) on $\bar{\ell}_4$, which need only be satisfied at $M_\pi^{\max}$ for the ξ-expansion to hold, the minimum of the bound on c_F in the region $M_\pi \in [0, M_\pi^{\max}]$ must be found and imposed as an upper bound on c_F. Thus,

$$c_F \leq \min_{M_\pi \in [0,\, M_\pi^{\max}]} \left\{ \frac{1}{4}\left[\ln\left(\frac{\Omega_F}{M_\pi^2}\right)^2\right]^2 - \left(\frac{4\pi F}{M_\pi}\right)^2 r_+^2 \left[r_+^2 - r_+ - C\right] \right\} , \tag{24}$$

with r_+ given above. This bound is very sensitive to the values of the LECs, and is not very enlightening when LO and NLO LECs, such as those given in Table 4 are used, assuming no correlations between them. However, for a given fit, this bound may be quite constraining. Thus, we impose this upper bound and the lower bound on $\bar{\ell}_4$ given in Eq. (23) when fitting lattice results to NNLO ξ-expansion expressions.

The fixed-order bounds on LECs discussed above are mainly of technical use here: they are enforced to avoid that the fitting routine gets lost in exploring unphysical regions of parameter space. However, for theories other than QCD which have $SU(2)$ χPT as a low-energy description, one could imagine being in a situation where these bounds suggest a failure of the effective theory in a region of pion masses where it is not entirely clear what is meant by the requirement that chiral corrections are "small".

For completeness we also provide here the analytical expression for the physical F_π solution of the NNLO expression for F in Eq. (7). It is given by [48]:

$$F_\pi = F\left\{\frac{1}{4} + S + \frac{1}{2}\sqrt{-4S^2 - 2p + \frac{q}{S}}\right\} , \tag{25}$$

with

$$p = -\frac{3}{8} - C \tag{26}$$

$$q = \frac{1}{8} + \frac{C}{2} , \tag{27}$$

and

$$S = \frac{1}{2}\sqrt{-\frac{2}{3}p + \frac{1}{3}(Q + \frac{\Delta_0}{Q})} \tag{28}$$

$$Q = \left[\frac{\Delta_1 + \sqrt{\Delta_1^2 - 4\Delta_0^3}}{2}\right] , \tag{29}$$

where

$$\Delta_0 = C^2 - 12D \tag{30}$$

$$\Delta_1 = -2C^3 - 27D - 72CD . \tag{31}$$

References

[1] S. Durr, Z. Fodor, J. Frison, C. Hoelbling, R. Hoffmann, et al., Ab initio determination of light hadron masses, Science 322 (2008) 1224–1227. arXiv:0906.3599, doi:10.1126/science.1163233.

[2] S. Aoki, et al., 2+1 Flavor Lattice QCD toward the Physical Point, Phys.Rev. D79 (2009) 034503. arXiv:0807.1661, doi:10.1103/PhysRevD.79.034503.

[3] S. Aoki, et al., Physical Point Simulation in 2+1 Flavor Lattice QCD, Phys.Rev. D81 (2010) 074503. arXiv:0911.2561, doi:10.1103/PhysRevD.81.074503.

[4] S. Durr, Z. Fodor, C. Hoelbling, S. Katz, S. Krieg, et al., Lattice QCD at the physical point: light quark masses, Phys.Lett. B701 (2011) 265–268. arXiv:1011.2403, doi:10.1016/j.physletb.2011.05.053.

[5] S. Durr, Z. Fodor, C. Hoelbling, S. Katz, S. Krieg, et al., Lattice QCD at the physical point: simulation and analysis details, JHEP 1108 (2011) 148. arXiv:1011.2711, doi:10.1007/JHEP08(2011)148.

[6] S. Borsanyi, S. Durr, Z. Fodor, S. Krieg, A. Schafer, et al., SU(2) chiral perturbation theory low-energy constants from 2+1 flavor staggered lattice simulations, Phys.Rev. D88 (2013) 014513. arXiv:1205.0788, doi:10.1103/PhysRevD.88.014513.

[7] R. Arthur, et al., Domain Wall QCD with Near-Physical Pions, Phys.Rev. D87 (2013) 094514. arXiv:1208.4412, doi:10.1103/PhysRevD.87.094514.

[8] A. Bazavov, et al., Lattice QCD ensembles with four flavors of highly improved staggered quarks, Phys.Rev. D87 (2013) 054505. arXiv:1212.4768, doi:10.1103/PhysRevD.87.054505.

[9] S. Weinberg, Phenomenological Lagrangians, Physica A96 (1979) 327.

[10] J. Gasser, H. Leutwyler, Chiral Perturbation Theory to One Loop, Annals Phys. 158 (1984) 142. doi:10.1016/0003-4916(84)90242-2.

[11] G. Colangelo, S. Durr, A. Juttner, L. Lellouch, H. Leutwyler, et al., Review of lattice results concerning low energy particle physics, Eur.Phys.J. C71 (2011) 1695. arXiv:1011.4408, doi:10.1140/epjc/s10052-011-1695-1.

[12] G. Colangelo, J. Gasser, H. Leutwyler, pi pi scattering, Nucl.Phys. B603 (2001) 125–179. arXiv:hep-ph/0103088, doi:10.1016/S0550-3213(01)00147-X.

[13] C. Allton, et al., Physical Results from 2+1 Flavor Domain Wall QCD and SU(2) Chiral Perturbation Theory, Phys.Rev. D78 (2008) 114509. arXiv:0804.0473, doi:10.1103/PhysRevD.78.114509.

[14] A. Bazavov, et al., MILC results for light pseudoscalars, PoS CD09 (2009) 007. arXiv:0910.2966.

[15] Y. Aoki, et al., Continuum Limit Physics from 2+1 Flavor Domain Wall QCD, Phys.Rev. D83 (2011) 074508. arXiv:1011.0892, doi:10.1103/PhysRevD.83.074508.

[16] A. Bazavov, et al., Results for light pseudoscalar mesons, PoS LATTICE2010 (2010) 074. arXiv:1012.0868.

[17] A. Bazavov, C. Bernard, C. DeTar, X. Du, W. Freeman, et al., Staggered chiral perturbation theory in the two-flavor case and SU(2) analysis of the MILC data, PoS LATTICE2010 (2010) 083. arXiv:1011.1792.

[18] S. Beane, W. Detmold, P. Junnarkar, T. Luu, K. Orginos, et al., SU(2) Low-Energy Constants from Mixed-Action Lattice QCD, Phys.Rev. D86 (2012) 094509. arXiv:1108.1380, doi:10.1103/PhysRevD.86.094509.

[19] R. Baron, P. Boucaud, J. Carbonell, A. Deuzeman, V. Drach, et al., Light hadrons from lattice QCD with light (u,d), strange and charm dynamical quarks, JHEP 1006 (2010) 111. arXiv:1004.5284, doi:10.1007/JHEP06(2010)111.

[20] R. Baron, et al., Light hadrons from Nf=2+1+1 dynamical twisted mass fermions, PoS LATTICE2010 (2010) 123. arXiv:1101.0518.

[21] L. Del Debbio, L. Giusti, M. Luscher, R. Petronzio, N. Tantalo, QCD with light Wilson quarks on fine lattices (I): First experiences and physics results, JHEP 0702 (2007) 056. arXiv:hep-lat/0610059, doi:10.1088/1126-6708/2007/02/056.

[22] J. Noaki, et al., Convergence of the chiral expansion in two-flavor lattice QCD, Phys. Rev. Lett. 101 (2008) 202004. arXiv:0806.0894, doi:10.1103/PhysRevLett.101.202004.

[23] R. Frezzotti, V. Lubicz, S. Simula, Electromagnetic form factor of the pion from twisted-mass lattice QCD at $N_f = 2$, Phys. Rev. D79 (2009) 074506. arXiv:0812.4042, doi:10.1103/PhysRevD.79.074506.

[24] S. Aoki, et al., Pion form factors from two-flavor lattice QCD with exact chiral symmetry, Phys. Rev. D80 (2009) 034508. arXiv:0905.2465, doi:10.1103/PhysRevD.80.034508.

[25] R. Baron, et al., Light meson physics from maximally twisted mass lattice QCD, JHEP 08 (2010) 097. arXiv:0911.5061, doi:10.1007/JHEP08(2010)097.

[26] T.-W. Chiu, T.-H. Hsieh, Y.-Y. Mao, Pseudoscalar Meson in Two Flavors QCD with the Optimal Domain-Wall Fermion, Phys.Lett. B717 (2012) 420–424. arXiv:1109.3675, doi:10.1016/j.physletb.2012.09.067.

[27] F. Bernardoni, N. Garron, P. Hernandez, S. Necco, C. Pena, Light quark correlators in a mixed-action setup, PoS LATTICE2011 (2011) 109. arXiv:1110.0922.

[28] R. Horsley, Y. Nakamura, A. Nobile, P. Rakow, G. Schierholz, et al., Nucleon axial charge and pion decay constant from two-flavor lattice QCDarXiv:1302.2233.

[29] B. B. Brandt, A. Juttner, H. Wittig, The pion vector form factor from lattice QCD and NNLO chiral perturbation theoryarXiv:1306.2916.

[30] P. Weisz, Continuum Limit Improved Lattice Action for Pure Yang-Mills Theory. 1., Nucl.Phys. B212 (1983) 1, erratum-ibid. B247 (1984) 544. doi:10.1016/0550-3213(83)90595-3.

[31] P. Weisz, R. Wohlert, Continuum Limit Improved Lattice Action for Pure Yang-Mills Theory. 2., Nucl.Phys. B236 (1984) 397. doi:10.1016/0550-3213(84)90543-1.

[32] M. Luscher, P. Weisz, On-Shell Improved Lattice Gauge Theories, Commun.Math.Phys. 97 (1985) 59. doi:10.1007/BF01206178.

[33] M. Luscher, P. Weisz, Computation of the Action for On-Shell Improved Lattice Gauge Theories at Weak Coupling, Phys.Lett. B158 (1985) 250. doi:10.1016/0370-2693(85)90966-9.

[34] B. Sheikholeslami, R. Wohlert, Improved Continuum Limit Lattice Action for QCD with Wilson Fermions, Nucl.Phys. B259 (1985) 572. doi:10.1016/0550-3213(85)90002-1.

[35] A. Hasenfratz, F. Knechtli, Flavor symmetry and the static potential with hypercubic blocking, Phys.Rev. D64 (2001) 034504. arXiv:hep-lat/0103029, doi:10.1103/PhysRevD.64.034504.

[36] C. Morningstar, M. J. Peardon, Analytic smearing of SU(3) link variables in lattice QCD, Phys.Rev. D69 (2004) 054501. arXiv:hep-lat/0311018, doi:10.1103/PhysRevD.69.054501.

[37] S. Capitani, S. Durr, C. Hoelbling, Rationale for UV-filtered clover fermions, JHEP 0611 (2006) 028. arXiv:hep-lat/0607006, doi:10.1088/1126-6708/2006/11/028.

[38] S. Durr, Z. Fodor, C. Hoelbling, S. Katz, S. Krieg, et al., Precision computation of the kaon bag parameter, Phys.Lett. B705 (2011) 477–481. arXiv:1106.3230, doi:10.1016/j.physletb.2011.10.043.

[39] G. Heatlie, G. Martinelli, C. Pittori, G. Rossi, C. T. Sachrajda, The improvement of hadronic matrix elements in lattice QCD, Nucl.Phys. B352 (1991) 266–288. doi:10.1016/0550-3213(91)90137-M.

[40] R. Arthur, P. Boyle, Step Scaling with off-shell renormalisation, Phys.Rev. D83 (2011) 114511. arXiv:1006.0422, doi:10.1103/PhysRevD.83.114511.

[41] G. Martinelli, C. Pittori, C. T. Sachrajda, M. Testa, A. Vladikas, A General method for nonperturbative renormalization of lattice operators, Nucl.Phys. B445 (1995) 81–108. arXiv:hep-lat/9411010, doi:10.1016/0550-3213(95)00126-D.

[42] K. Chetyrkin, A. Retey, Renormalization and running of quark mass and field in the regularization invariant and MS-bar schemes at three loops and four loops, Nucl.Phys. B583 (2000) 3–34. arXiv:hep-ph/9910332, doi:10.1016/S0550-3213(00)00331-X.

[43] J. Gasser, H. Leutwyler, Light Quarks at Low Temperatures, Phys.Lett. B184 (1987) 83. doi:10.1016/0370-2693(87)90492-8.

[44] G. Colangelo, S. Durr, C. Haefeli, Finite volume effects for meson masses and decay constants, Nucl.Phys. B721 (2005) 136–174. arXiv:hep-lat/0503014, doi:10.1016/j.nuclphysb.2005.05.015.

[45] L. Lellouch, Kaon physics: A Lattice perspective, PoS LATTICE2008 (2009) 015. arXiv:0902.4545.

[46] J. Beringer, et al., Review of Particle Physics (RPP), Phys.Rev. D86 (2012) 010001. doi:10.1103/PhysRevD.86.010001.

[47] G. Colangelo, et al., Review of lattice results concerning low energy particle physics, [Online, 25 July 2013].
URL http://itpwiki.unibe.ch/flag/index.php/Review_of_lattice_results_concerning_low_energy_particle_physics

[48] Wikipedia, Quartic function — Wikipedia, the free encyclopedia, [Online; accessed 24 July 2012, 12:39 UTC] (2012).
URL http://en.wikipedia.org/w/index.php?title=Quartic_function&oldid=569041825